Microfluidics for bacterial chemotaxis†

Tanvir Ahmed,[a] Thomas S. Shimizu[b] and Roman Stocker*[a]

Received 1st June 2010, Accepted 11th August 2010
DOI: 10.1039/c0ib00049c

Microfluidics is revolutionizing the way we study the motile behavior of cells, by enabling observations at high spatial and temporal resolution in carefully controlled microenvironments. An important class of such behavior is bacterial chemotaxis, which plays a fundamental role in a broad range of processes, including disease pathogenesis, biofilm formation, bioremediation, and even carbon cycling in the ocean. In biophysical research, bacterial chemotaxis represents a powerful model system to understand how cells and organisms sense and respond to gradients. Using microfluidics to study chemotaxis of free-swimming bacteria presents experimental challenges that are distinct from those arising in chemotaxis studies of surface-adherent cells. Recently, these challenges have been met by the development of advanced microdevices, able to generate flow-free, steady gradients of arbitrary shape. Much attention to date has been focused on tool development. Yet, we are now at an exciting turning point where science begins to balance technology. Indeed, recent microfluidic studies provided new insights on both the mechanisms governing bacterial gradient sensing (*e.g.* tuning of response sensitivity, discrimination between conflicting gradients) and the large-scale consequences of chemotaxis (*e.g.* in the oceans). Here we outline the principles underlying recently proposed gradient generators for bacterial chemotaxis, illustrate the advantage of the microfluidic approach through selected examples, and identify a broader set of scientific questions that may now be addressed with this rapidly developing technology. The latest generation of microfluidic gradient generators, in particular, holds appeal for both biophysicists seeking to unravel the fundamental mechanisms of bacterial chemotaxis, and ecologists wishing to model chemotaxis in realistic environments. Time is ripe for a deeper integration between technology and biology in fully bringing to bear microfluidics on studies of this fascinating microbial behavior.

1. Bacterial chemotaxis: sample applications

Chemotaxis is the ability of organisms to sense gradients in their chemical environment and adjust their motile behavior accordingly. Bacteria, for example, are often able to measure chemical gradients and move towards higher concentrations of a favorable chemical or lower concentrations of an unfavorable one. An early reported example of such behavior was aerotaxis, discovered by Engelmann in 1881. While pursuing experiments on photosynthesis, he observed bacteria actively migrating towards regions of higher oxygen concentration generated by algal cells.[1] Bacterial chemotaxis has been the subject of ever-increasing scientific interest in the past five decades, ever since systematic and quantitative methods for studying chemotaxis were introduced, beginning in the 1960s. On the one hand, it has received much attention as a biological sensory system that is tractable at the molecular level in genetically well defined and manipulatable model organisms (see next section). On the other hand, its study has found

[a] *Ralph M. Parsons Laboratory, Department of Civil and Environmental Engineering, Massachusetts Institute of Technology, Building 48, Room 335, 77 Massachusetts Ave, Cambridge, MA 02139, USA. E-mail: romans@mit.edu; Tel: +1 617 253 3726*
[b] *FOM Institute for Atomic and Molecular Physics (AMOLF), Science Park 104, 1098 XG Amsterdam, The Netherlands*
† Published as part of a themed issue on Mechanisms of Directed Cell Migration: Guest Editors David Beebe and Anna Huttenlocher.

Insight, innovation, integration

Insight. This manuscript shows that microfluidic technology is ideally suited to study bacterial chemotaxis. Recent findings from microfluidic studies have provided novel insight on both the fundamental mechanisms by which bacteria sense gradients (*e.g.* logarithmic sensing, fold-change-detection in *E. coli*) and the pervasive occurrence and ecological importance of bacterial chemotaxis in specific environments (*e.g.* the oceans). **Innovation**. These novel insights into bacterial chemotaxis stemmed from the ability of microfluidic technology to (i) generate carefully controlled gradients and (ii) enable observations at high spatial and temporal resolution. **Integration**. The primary challenge in this field lies in a more widespread integration between technology and biology. Important advances in our understanding of bacterial chemotaxis are just ahead of us, as the field is reaching a balance between the development of new techniques and their application to cutting-edge biological questions.

practical applications in a wide range of fields. We briefly summarize in this section a handful of these applications as examples, with a focus on bacterial-host interactions and the transformation of dissolved matter. Our aim is not to provide a comprehensive overview, but to relay some sense of the breadth of processes that involve bacterial chemotaxis.

In pathogenesis, many bacteria use chemotaxis to find suitable colonization sites. For example, chemotaxis can guide *Helicobacter pylori* (the primary causative agent of chronic gastric diseases) to the mucus lining of the human stomach,[2] *Campylobacter jejuni* (one of the major factors in food-borne diseases) towards bile and mucin in the human gallbladder and intestinal tract,[3] *Vibrio cholerae* towards the intestinal mucosa,[4] pathogenic enterohemorrhagic *Escherichia coli* to epithelial cells in the human gastrointestinal tract,[5] free-living *Vibrio anguillarium* from seawater to the skin of fish,[6] and *Agrobacterium tumefaciens* towards plant wounds.[7] In many of these cases, chemotaxis can result in increased rates of host infection.

In the wider natural environment, chemotaxis affects the processing and cycling of elements by guiding bacteria towards and away from chemicals in diverse settings. Around plant roots, chemotaxis can guide free-living soil bacteria, for example those belonging to the Rhizobium species, to legume root hairs, favoring nitrogen fixation.[8] In the subsurface, chemotaxis can guide *Pseudomonas putida* and other species towards harmful organic compounds, facilitating the bio-remediation of contaminated sites.[9] In the ocean, chemotaxis allows bacteria to effectively utilize ephemeral resource hotspots, increasing the rate at which limiting elements are recycled and contributing to shape trophic interactions,[10–13] thereby potentially enhancing productivity levels and bio-geochemical fluxes.[14–16]

In all these cases, a better understanding of the rates and roles of chemotaxis will strongly benefit from the ability to perform systematic experiments in controlled microenvironments. A great deal could be learned by either reproducing realistic environments experienced by bacteria in nature, or by designing artificial ones that can inform on the molecules and mechanisms underlying chemotactic behavior. Microfluidics represents a powerful, convenient and versatile approach in both cases. As this review attempts to highlight, the challenge now is to move decisively beyond technology development and proof of concept experiments, and more deeply bring to bear microfluidics on the vast range of fundamental questions on bacterial chemotaxis that await exploration.

2. Bacterial chemotaxis: fundamentals

At the cellular level, bacterial chemotaxis can be understood as a biased random walk in three-dimensional space.[17] Motile cells constantly sample their local environment by propelling themselves using one or more helical flagella in a direction that is determined by chance. In an isotropic environment, this random motility allows cells to explore space much more

Tanvir Ahmed

Tanvir Ahmed is a PhD candidate in Civil and Environmental Engineering at the Massachusetts Institute of Technology, where he has been working in Roman Stocker's Environmental Microfluidics Group since 2005. His research interests focus on the application of microfluidic techniques to the study of microbial processes, with an emphasis on bacterial chemotaxis, behavioral adaptation of marine microbes, and microbial predator-prey dynamics. Tanvir Ahmed received his BSc and MSc from the Bangladesh University of Engineering and Technology (BUET) in 2003 and 2005, respectively, and served as a lecturer at BUET from 2003 to 2005.

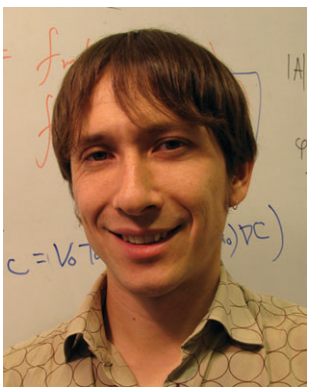

Thomas S. Shimizu

Tom Shimizu received his PhD from the University of Cambridge in 2003, working on biophysical problems of intracellular signaling using stochastic methods. In 2002–2003, he spent a year as a research lecturer at Keio University, before taking up a postdoctoral fellowship at Harvard University, where he worked on Förster resonance energy transfer (FRET) experiments in live bacteria. In 2009, he joined the FOM Institute for Atomic and Molecular Physics (AMOLF) to start a new research group focusing on the physics of cell signaling and behavior.

Roman Stocker

Roman Stocker is an Associate Professor of Civil and Environmental Engineering at the Massachusetts Institute of Technology, where he has served on the faculty since 2005. He received his BSc and PhD in Civil Engineering from the University of Padova (Italy) in 1998 and 2002, respectively, and held an Instructor position in Applied Mathematics at MIT from 2002 to 2005. He currently leads the Environmental Microfluidics Group at MIT, which focuses on integrating microfluidic technology and theoretical approaches to further our understanding of micro-scale environmental processes. A primary emphasis of his research is on microbial processes in the ocean.

efficiently than they would if they were to spread by Brownian motion alone. In the presence of a spatial gradient of chemoeffectors, a sensory system imposes a bias on this random behavior in a manner that yields net migration in a favorable direction, *i.e.* either towards higher concentrations of attractants, or lower concentrations of repellents. The details of the machinery for both motility and sensing are as diverse as the species that demonstrate these behaviors and their respective habitats—chemotaxis is observed throughout all major prokaryotic lineages, including the archea—but there are also highly conserved design features at the molecular level.[18,19] The basic paradigm established in studies of the model organism *E. coli*[20] thus serves as a guide for exploring the plethora of possible variations on this theme.

E. coli propels itself by rotating multiple helical filaments which are anchored to the cell wall by ion-driven molecular motors. When all motors rotate counterclockwise (looking from the distal end of the filament, toward the cell), the left-handed helical filaments coalesce into a coherent bundle yielding relatively straight trajectories, called "runs". When one or more of the motors reverses direction, the bundle is disrupted, yielding brief, erratic reorientation events, called "tumbles". Thus, the random-walk behavior of each cell can be described as a two-state sequence, consisting of runs and tumbles. The sensory system controlling this behavior responds to chemical cues by modulating the fraction of time spent in each of these two states.

The dynamics of the sensory response is crucial for effective chemotaxis, as the signaling pathway must respond on time scales that match the otherwise random motile behavior. When receptors at the cell surface bind chemoeffector molecules, they excite a network of chemical reactions that results in a motor response within a few hundred milliseconds.[21,22] This is much shorter than the average duration of runs, which are typically around 1 s in the absence of chemoeffector gradients, but can extend beyond 10 s when swimming up steep gradients. Gradient sensing is achieved by temporal comparisons, in which the receptor occupancy in the recent past is compared to that in the more distant past.[23] This comparison is mediated by a chemical "memory"—a reversible covalent modification of receptors, which counteracts the effect of bound chemoeffectors, leading to adaptation on a slower time scale ($\sim$10 s) than the excitatory response. This adaptation time scale roughly matches the average time over which swimming directions are decorrelated during runs (although swimming trajectories during runs are smooth, they are never perfectly straight, due to the asymmetric cell body, which introduces a wobble in the trajectory, and Brownian rotational diffusion, which induces a random component to the swimming direction).[17] The steepness of gradients that can be sensed are thus determined by the swimming speed ($\sim$30 μm s^{-1} in *E. coli*), which converts the spatial gradient into a temporal one, and the time scales of the chemical reactions underlying this sensory response.

Because of its relative simplicity, this signal transduction pathway is among the best characterized signaling systems in biology. Much recent work has focused on how this pathway achieves important physiological functions, such as precise adaptation,[24,25] signal amplification[26,27] and temporal gradient sensing,[28,29] but many open questions remain in how these properties combine as a control strategy for migrating cell populations, as highlighted by a series of theoretical studies on the topic.[30–36] Following a decade of relative silence after the earlier theoretical work,[30,37] recent years have seen a spur of papers addressing questions of how intracellular signaling can affect the behavior of migrating cells and populations.[30–36]

There is a sense that time is ripe to study the design of such cellular control circuits and their molecular underpinnings, given the large amount of information now available about the underlying molecules and the rich set of experimental tools to probe the mechanisms further. The quantitative control over spatial chemoeffector gradients made possible by microfluidic devices holds great promise for probing such questions.

While *E. coli* represents the best-studied model system of bacterial motility and chemotaxis, a wide range of other motility strategies exists among bacteria. Here, we provide selected examples to give an overview of the time and velocity scales associated with bacterial motility. Two widely studied species that have a motility pattern closely related to that of *E. coli* are *Bacillus subtilis* and *Salmonella typhimurium*, both peritrichously flagellated bacteria that swim in a run and tumble fashion. The former swims at $\sim$30 μm s^{-1},[38] the latter at 29–55 μm s^{-1}.[39] Similar speeds (22–33 μm s^{-1})[40] are also exhibited by *Helicobacter pylori*, which uses 2–6 unipolar flagella to swim and chemotax in the human stomach.

On the other hand, considerably larger speeds and markedly different swimming strategies compared to *E. coli* have been frequently reported (see Mitchell and Kogure[41]). For example, monotrichous (*i.e.* having a single polar flagellum) bacteria and many marine bacteria swim using a run and reverse strategy. The bacterium *Vibrio alginolyticus*, native to both aquatic and marine environments, can swim in this manner, at speeds of 77–116 μm s^{-1}.[39] Marine bacteria isolated from the coastal ocean and of size comparable to *E. coli*, including *Pseudoalteromonas haloplanktis*, also swim using run and reverse motility, at speeds exceeding 400 μm s^{-1},[42] an order of magnitude faster than *E. coli*. The speed record, however, currently belongs to marine bacteria isolated from the water–sediment interface, where Candidatus *Ovibacter propellens* swims at up to 1000 μm s^{-1}.[43] The difference in swimming speed suggests also a difference in the signal processing time in reacting to gradients. Segall *et al.*[21] suggested that a response time of 200 ms is sufficiently fast for *E. coli* to react to sensed gradients before being reoriented by Brownian rotational diffusion. Mitchell *et al.*[42] suggested that this is not a lower limit and that a processing time of as little as a few milliseconds will be necessary for bacteria swimming at 400 μm s^{-1}.

Bacteria from the sediment–water interface are often considerably larger than *E. coli*. For example, *Thiovulum majus* is up to 25 μm in size and because Brownian rotational diffusion scales with the inverse of the cube of bacterial size, these larger bacteria are considerably more effective at determining their swimming direction and their motility pattern has been denoted as 'steering'.[44]

Yet other species swim in a run and stop mode (*e.g. Rhodobacter sphaeroides*[45]). In many cases, very little or no information is available on the chemotactic preferences and the chemotactic pathways of these organisms.

In recent years, a number of microfluidic studies on the motility and chemotaxis of bacterial species other than *E. coli* have appeared.[12,13,46–49] Yet much of the diversity in the swimming strategies and response time scales among the bacteria outlined above, remains only roughly characterized. Quantitative studies of such less well-characterized species considerably increases the breadth of potential applications of microfluidic devices as assays to study motility and chemotaxis under highly controlled conditions.

3. Bacterial chemotaxis assays prior to the advent of microfluidics

Chemotaxis assays have been used for more than four decades to quantify the preference of bacteria for a given chemical and the rates of their chemotactic motility in chemical gradients. The first quantitative bacterial chemotaxis assay was the capillary assay, developed by Julius Adler in the 1960s.[50] Several other assays have been developed since, including stopped-flow diffusion chambers (SFDC),[51] continuous-flow capillary assays,[52] two-chamber glass capillary arrays,[53] swarm plate assays,[54] tethered cell assays,[55] and automated tracking of swimming cells.[17] Excellent reviews of most of these assays can be found in Jain *et al.*[56] and Englert *et al.*[57] Here we briefly describe some salient features, for comparison with the microfluidic techniques presented in the following sections.

The basic operation of the capillary assay involves immersing a chemoeffector-filled capillary tube in a bacterial suspension and allowing the bacteria to sense and respond to the chemical gradient that forms near the mouth of the capillary by swimming into the capillary, as the chemical diffuses into the suspension.[50] The quantification of the bacterial response occurs by counting bacteria in the capillary after serial dilution and plating.

Exposure of a bacterial population to a transient, diffusing chemoeffector gradient is also the operating principle behind several subsequent assays. SFDC assays rely on suddenly stopping two impinging streams of a bacterial suspension that differ only in chemoeffector concentration.[51,58] The distribution of bacteria along the evolving gradient is measured by light-scattering techniques, bypassing the need for the time-consuming plate counting characteristic of capillary assays, but still limiting resolution to population-scale measurements.

Swarm plate assays are based on inoculating a bacterial population on a semisolid agar plate made with metabolizable chemoattractant.[54] As bacteria gradually metabolize the chemoattractant, they create radial chemoattractant gradients that trigger their outward migration in characteristic rings. The rate at which the diameter of this ring increases provides a (rather coarse) measure of chemotaxis, and swarm plate assays are often used primarily at a qualitative level.

Considerably more detailed information is provided by single-cell approaches, such as the temporal stimulation of tethered cells[55] and the three-dimensional tracking of individual bacteria in chemoeffector gradients.[17] These techniques are among the most sophisticated approaches, and in several aspects (*e.g.* the 3D tracking) remain largely unparalleled even by more modern methods. They have revealed fundamental mechanistic aspects of chemotaxis, enabling the quantification of run lengths, tumble frequencies and adaptation responses that paved the way for formulating theoretical models of bacterial chemotaxis.[30–32,34–36,59]

All of these assays, developed before microfluidic technology, have yielded invaluable information on bacterial chemotaxis. There is little doubt that some of these techniques will continue to be used in many laboratories, whether it be for historical reasons, or because of the simplicity and/or convenience of the setup (*e.g.* capillary assays, swarm plates). Quantitative and rigorous characterization of bacterial motility is difficult to achieve with many of these techniques, however, and those that are amenable to quantitative analysis tend to be more difficult to implement, or laborious. Perhaps the most important and general difficulty in these bacterial chemotaxis assays that predate microfluidics arises when accurate characterization of chemoeffector gradients are desired. Both capillary assays and SFDCs have largely relied on mathematical modeling, rather than direct observation, to quantify chemoeffector gradients, but even small disturbances can significantly perturb or entirely disrupt gradients.[60] Furthermore, while some techniques provide single-cell observations (see above), many (*e.g.* capillary assays, swarm plates) measure the bacterial response only at the population level, with considerable uncertainty due to measurement techniques. Microfluidic technology offers the possibility to overcome these limitations by enabling generation of highly controlled chemical gradients and measurements of the bacterial response at high spatio-temporal resolution.

4. Advantages of a microfluidic approach to study bacterial chemotaxis

Microfluidics has become an important platform for biological research in a wide range of fields, spanning from cell biology to disease diagnostics and microbial community dynamics[61,62] owing to the unprecedented degree of control it offers over the chemical and physical environments of cells at the microscale. We highlight two main features that make microfluidic devices advantageous for the study of bacterial chemotaxis.

Firstly, the accurate control over channel geometries and fluid flow, combined with significant levels of automation in operation, provide an appealing strategy for controlling experiments involving gradients on a scale suitable for bacterial studies. Because of the low Reynolds number of most microfluidic flows, turbulence is absent and chemical gradients are smooth, straightforward to predict mathematically from the solution of the advection-diffusion equation. Therefore it enables one to generate precise concentration gradients and systematically explore a wide range of parameters.

Secondly, the size and transparency of microchannels are ideally suited for accurately measuring the concentration gradients as well as observing the bacterial response to the gradients by microscopy. Automated cell-counting by video-microscopy and image analysis ensure excellent statistics on cell distributions. Furthermore, bacterial chemotaxis can be observed directly at the scale of the individual organism, by tracking single cells over time in well-defined chemoeffector gradients. Coupled with computer-controlled microscopy, this

Table 1 Metrics of bacterial chemotaxis. This table provides a concise overview of different metrics used to quantify bacterial chemotaxis, both at the population scale and at the single-cell scale.

1. POPULATION-SCALE METRICS OF CHEMOTAXIS

1A. Chemotactic Sensitivity Coefficient, χ_0. A population-scale measure of the strength of attraction of a given strain towards a chemoeffector. It arises from the bacterial transport equation, which in one dimension reads:

$$\frac{\partial B}{\partial t} = \frac{\partial}{\partial x}\left(\mu \frac{\partial B}{\partial x}\right) - \frac{\partial}{\partial x}(V_C B);\ V_C = \frac{8\nu_{2D}}{3\pi}\tanh\left(\frac{\chi_0 \pi}{8\nu_{2D}}\frac{K_D}{(K_D + C)^2}\frac{\mathrm{d}C}{\mathrm{d}x}\right)$$

where $B(x,t)$ is the bacterial concentration, μ is the random motility coefficient, v_{2D} is the two-dimensional projection of the bacterial swimming speed, C is the chemoeffector concentration, K_D is the chemoreceptor-ligand dissociation constant, and V_C is the chemotactic velocity (see below). (ref. 7, 73 and 96).

1B. Chemotaxis Index, I_C and Hot Spot Index, H. Two indicators that measure the strength of chemotaxis from the magnitude of the accumulation of a population within a certain region, relative to background levels. Both were used in studies with the nutrient pulse generator. I_C was determined as the mean cell concentration over the central 600 μm (ref. 12, 46–48 and 86). H was similarly defined, except for the central 300 μm (ref. 13). Large I_C and H values indicate strong accumulation, while $I_C = 1$ and $H = 1$ corresponds to a uniform cell distribution (*i.e.* no chemotaxis).

1C. Chemotaxis Migration Coefficient, CMC. A measure of the distance that cells travel from the middle of the channel in a certain direction under a chemoeffector gradient. It is computed as CMC $= \int xB(x)\mathrm{d}x/(w/2)$, where $B(x)$ is the cell concentration (normalized to a mean of 1), x is the direction across the channel (*i.e.* along the gradient), with $x = 0$ at mid-width, and the integral extends over the entire width of the channel, w. No chemotaxis (uniform distribution) corresponds to CMC $= 0$, while accumulation towards $x > 0$ corresponds to CMC > 0. (ref. 5, 70, 90, 92 and 95).

2. SINGLE-CELL BASED METRICS OF CHEMOTAXIS

2A. Migration Index, MI. A measure based on the relative occurrence of cells moving up and down the gradient. Denoting as f^+ (f^-) the number of velocity data points up (down) the gradient, MI $= (f^+ - f^-)/(f^+ + f^-)$. In general, $-1 \leq$ MI ≤ 1. Larger values of MI indicate stronger chemotaxis. We note that MI does not correspond to cell flux, because only the number of velocity data points, not the velocities themselves, are considered. (ref. 87).

2B. Chemotactic velocity, V_C. The mean drift velocity along a chemoeffector gradient. It can be computed at the population level (see 1A), but also directly at the single-cell level, as $V_C = (8v_{2D}/3\pi)(T^- - T^+)/(T^+ + T^-)$, where, T^+ (T^-) is the average run-time of cells up (down) the gradient and v_{2D} is the two-dimensional projection of the bacterial swimming speed. Unlike the Migration Index, V_C is based on the calculation of cell fluxes, and is thus a more appropriate measure of chemotaxis when velocities are not constant. (ref. 7, 59).

makes for a versatile platform to acquire data of unprecedented quality and quantity in experiments on bacterial chemotaxis.

Chemoeffector concentration profiles can be conveniently quantified by using tracer dyes. Use of fluorescent tracer dyes enables one to simultaneously visualize the chemoeffector concentration field and the bacteria (*e.g.* by imaging unlabeled bacteria in phase contrast, or fluorescently labeled bacteria at a different wavelength). Commonly used tracer dyes include fluorescein, carboxyfluorescein and red rhodamine. Fluorescein has been shown not to adversely affect the chemotactic response of bacteria,[13] though this needs to be tested on a species-by-species basis for each dye. These dyes are useful as tracers because their diffusivities (*e.g.* 4.3×10^{-10} m^2 s^{-1} for fluorescein and rhodamine B at 25 °C[63]) are close to those of many low-molecular-weight solutes (*e.g.* 5.5×10^{-10} m^2 s^{-1} for α-methylaspartate[64]), hence their concentration field can be taken to represent that of the solute. Other dyes would have to be sought to represent concentration fields of chemoeffectors with significantly lower or higher diffusivity. Furthermore, the correspondence between dye and chemoeffector concentration breaks down in the case of metabolizable chemoeffectors, when bacteria consume a significant fraction of the chemoeffector over the course of the experiment. This effect can be minimized by working at low bacterial concentrations. Finally, non-fluorescent dyes such as trypan blue and food dyes are also commonly used and do not require a fluorescence detection setup for visualization. They are best used to quantify gradients separately from the chemotaxis experiments, since their use can interfere with the visualization of bacteria.

Data acquisition is typically achieved by videomicroscopy using a digital camera, with a microscope configured for phase-contrast imaging, fluorescence imaging, or both. Phase contrast imaging has the advantage that it can be applied to any bacterial species and is often used in microfluidic applications. It is particularly useful for studies of natural bacterial assemblages, where culturing is difficult and fluorescent tagging can be hard or undesirable. We predict this will represent a key benefit of the microfluidic approach in the near future, as environmental microbiologists are increasingly shifting focus from model organisms to natural assemblages. Fluorescence visualization has its advantages, but require that cells to be labeled, for example by genetic engineering to express Green Fluorescent Protein (GFP). Another potential concern with fluorescence imaging is the potentially disruptive effect of the fluorescence excitation light, which for many fluorophores contain significant power in the blue-green wavelengths to perturb chemotaxis.[65] Typical excitation power and exposure times required for fluorescence imaging in microfluidic chemotaxis assays are usually within the safe range, but it is advisable to ensure by appropriate control experiments that fluorescence excitation is not perturbing the chemotactic response or cell motility (these precautions carry over also to phase-contrast or any other type of imaging, where longpass filters are recommended for illumination for extended durations).

The bacterial response can be characterized at two levels: that of the population and that of the single cell. Spatial coordinates of individual bacteria can be conveniently extracted from acquired images by automated image analysis. Subtraction of a background image (*e.g.* the previous image in a sequence) facilitates cell identification by removing all non-moving objects, thus filtering out noise, speckles and attached cells from the resulting difference image. These coordinates are then used to construct spatial distribution profiles of bacteria, which can be used to compute various chemotactic response indices (see Table 1). In this manner, chemotaxis can be assessed at the population level. Additionally, cells can be tracked through a sequence of frames using particle-tracking software; provided the image-acquisition rate is high enough and the cell suspension is sufficiently dilute. The trajectories thus obtained yield information on swimming kinematics, including swimming speeds, turning angles/frequencies, and chemotactic velocities (see Table 1), allowing a quantification of chemotaxis at the single-cell level. The main limitation of cell tracking is imposed by the finite depth of field of the microscope, which only permits acquisition of relatively short segments of a bacterial trajectory before the cell swims out of focus. Although three-dimensional approaches have been proposed,[66] Berg's 3D tracking microscope[17] remains unmatched to this day as a 3D imaging technique for bacterial motility and chemotaxis.

As is common in pioneering applications of novel technologies, many microfluidic studies of bacterial chemotaxis to date have placed a dominant focus on technical innovations. Recent trends in the field, however, seem to signal the arrival at an exciting turning point, where novel and outstanding scientific questions are being addressed at an accelerating pace. The exposition of notable works provided below are not in strict chronological order, but highlight the salient steps in this path, with an emphasis on the trend towards scientific, rather than technological novelty. Extrapolating from this trajectory, we predict that the coming few years will see increasing numbers of novel, fundamental studies in bacterial chemotaxis enabled by microfluidic technology.

It is important to recognize that chemotaxis of free-swimming cells presents different fundamental challenges for the design of microfluidic devices and experiments from those presented by chemotaxis of surface-adherent cells. Gradients generated using laminar flows have been used extensively to study chemotaxis of surface-adherent cells.[67–69] Because streams of miscible fluids flowing side by side mix only by diffusion in microfluidic environments, gradients of arbitrary shape can be established by appropriately selecting the spatial layout and concentration of multiple adjacent streams. In this manner, flow along the microchannel establishes a gradient *across* the channel. Under steady flow rates, the gradient is steady at each location along the channel. This is convenient for surface-adherent cells, as they can be exposed to steady gradients with small shear forces (provided flow rates are small) and their migration will thus primarily be along the gradient.

Importantly, however, the shape of the gradient changes with distance along the flow in those devices. Hence, freely swimming cells such as bacteria would experience an unsteady gradient as they are transported along the microchannel by the flow. Although a significant number of microfluidic gradient generators for bacterial chemotaxis are flow-based, as discussed below, significant efforts have been made to establish flow-free gradients—in some cases achieving steadiness of the gradient—in order to avoid flow-induced mechanical perturbations and to follow the behavior of the same population of bacteria over time in a given field of view. The recent success of such devices represents in our view the most interesting methodological advance of microfluidic devices for bacterial chemotaxis.

In what follows, we distinguish between chemotaxis in flow-based and flow-free gradients. We further employ a second classification, that of steady *versus* unsteady gradients, since this distinction fundamentally affects how one performs chemotaxis experiments with bacteria, and what kind of tests can be performed.

5. Chemotaxis in a flowing environment

The earliest examples of microfluidic gradient generators for bacterial chemotaxis rely on flow to generate gradients. A number of configurations of flow-based devices have been developed.

Three-inlet parallel-flow device

The first such device was the three-inlet parallel-flow microchannel of Mao *et al.*[70] (Fig. 1A). This device is sometimes referred to as a "T-sensor", because of its resemblance to a T-shaped microfluidic device used to measure chemical concentrations,[71] and is reviewed in detail by Englert *et al.*[57] and Keenan *et al.*[71] Its operation is based on the confluence of three streams, joining into a single microchannel in a T-shaped configuration. One of the lateral streams contains a chemoeffector, while the opposite stream contains buffer. Diffusion between these two parallel streams generates a chemoeffector gradient across the microchannel. Bacteria are injected in the middle stream, in correspondence to the steepest part of the gradient. Chemotaxis can then be assessed as the preferential movement of cells towards the chemoeffector stream (Fig. 1B) and was quantified by Mao *et al.*[70] using the Chemotactic Migration Coefficient (see Table 1).

Mao *et al.*[70] used the three-inlet parallel-flow device to study chemotaxis of *E. coli* RP437. They found significant chemoattraction to 3.2 nM L-aspartate, nearly three orders of magnitude lower than the detection limit of capillary assays ($\sim$1 μM),[72] illustrating the high sensitivity that microfluidic devices can achieve. The authors further discovered a biphasic response to L-leucine (Fig. 1C), which is sensed by the Tar receptor as an attractant at low concentrations (1–100 μM) and by the Tsr receptor as a repellent at high concentrations (10 mM).

As for all flow-based gradient generators, the gradient experienced by bacteria in the three-inlet parallel-flow device as they are transported downstream by the flow is unsteady (Fig. 2A). The distribution of bacteria measured at the end of the channel thus results from their cumulative response to the evolving nonlinear gradient they experience during their journey along the microchannel. While this does not impair relative comparisons among experimental conditions, and

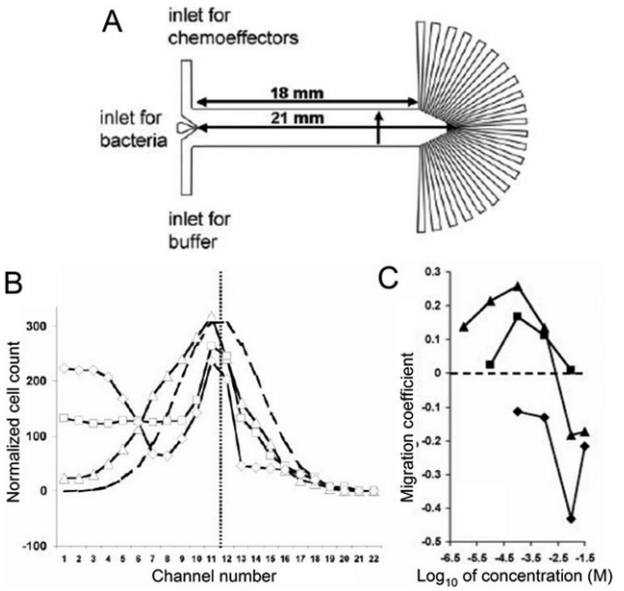

Fig. 1 The three-inlet parallel-flow device of Mao *et al.*[70] (A) Two streams from the outer inlet channels containing chemoeffector and buffer, respectively, converge upon entry to form parallel flows within a single channel that serves as the chemotaxis chamber. As they flow side by side, mixing due to diffusion results in a chemoeffector gradient across the chamber width. The middle inlet is used to inject bacteria, which experience a time-dependent gradient that is initially steep and step-like, where the two outer streams first meet, and gradually relaxes with distance as the cells flow downstream. The transverse distribution of bacteria across the chamber is obtained by counting cells partitioned into each of the 22 outlets. (B) The transverse distribution of *E. coli* RP437 exposed to a gradient of L-aspartate, for different concentrations of L-aspartate: 0 (dashed line), 3.2 nM (△), 10 nM (□), and 1 mM (◇). Channel numbers increase clockwise from the top in panel A. Chemotaxis results in an accumulation of cells towards the left. (C) Values of the Chemotaxis Migration Coefficient (see Table 1) of wild type (▲), serine-blind (■) and aspartate-blind (◆) *E. coli* cells to L-leucine. Notice the biphasic response of the wild type, which is attracted to low concentrations of L-leucine and repelled at high concentrations. (Reproduced from ref. 70. Copyright 2003 National Academy of Sciences, USA).

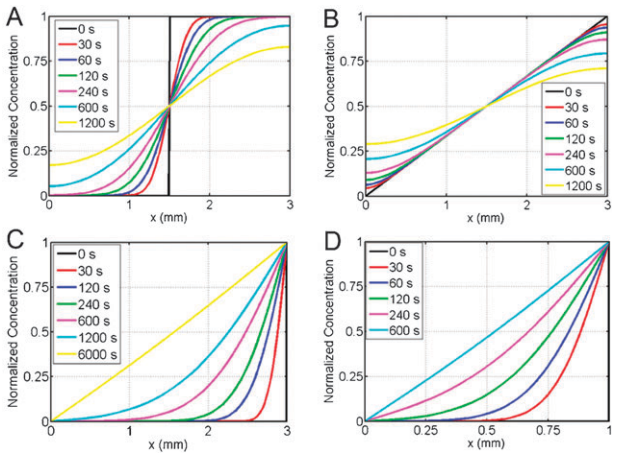

Fig. 2 Time evolution of concentration profiles in different gradient-generation approaches, obtained by numerical solution of the one-dimensional diffusion equation. In all panels, the horizontal coordinate x represents the distance transverse to the microchannel, and different curves correspond to the concentration profile at different times. For all cases the channel width $W = 3$ mm, except in (D), where $W = 1$ mm. (A) Initial step-like profile, often used in parallel-flow devices (ref. 70 and 73), evolving under no-flux boundary conditions. The latter are appropriate in general for flow-based and stopped-flow experiments, where the channel sidewalls (at $x = 0$ and $x = W$) are impermeable and thus allow no flux. In flow-based experiments, time corresponds to 'time in the flow' and is computed as the distance to the measurement point, divided by the mean flow speed. In stopped-flow experiments, time starts when the flow is stopped. Notice how, after 1–2 min, the profile is very different from the initial one, in view of the large flux due to the steep initial gradient. (B) Same as in A, but for a linear initial profile (*e.g.* ref. 5 and 87). The profile evolves more slowly, because the initial condition is a shallower gradient, which produces a smaller diffusive flux. (C) Relaxation towards a steady nonzero gradient, achieved by imposing constant-concentration boundary conditions, which apply to diffusion-based devices (ref. 97). The initial condition (zero concentration everywhere) evolves towards the linear profile that represents the steady-state solution to the one-dimensional diffusion equation. (D) Same as C, but with the channel width decreased three-fold. Notice the considerably (nine-fold) faster evolution of the gradient, due to the quadratic dependence of diffusion time on length (*e.g.* ref. 90–92, 95 and 96).

chemotaxis in unsteady gradients can itself be an interesting topic of investigation (see below), these complex and dynamic gradients can be confounding if quantitative characterizations of the underlying chemotactic mechanisms are desired. The departure from the initial concentration profile is particularly severe in this device because of the steepness of the initial gradient (Fig. 2A), which thus rapidly relaxes by diffusion. Fast experiments (*e.g.* rapid flow) partially alleviate this problem, but also reduce the time available for bacteria to respond.

Two-inlet parallel-flow device

A modification of the three-inlet parallel-flow device was proposed by Lanning *et al.*[73] Compared to the device of Mao *et al.*,[70] the two-inlet parallel-flow device uses only two parallel streams (Fig. 3A). Instead of being injected into the gradient from a separate stream, bacteria are contained in both streams, making for an initially uniform cell distribution across the channel. In contrast to most other microfluidic approaches, the bacterial distribution across the channel was measured by light scattering (Fig. 3B). The observed distribution was then fitted with the numerical solution of the bacterial transport equation[7] to compute the Chemotactic Sensitivity Coefficient[59] (see Table 1).

When operated under flow, this device exposes bacteria to an unsteady gradient (Fig. 2A) and mechanical forces due to the fluid flow, like the three-inlet parallel-flow device. Lanning *et al.*[73] performed an important comparison, by also operating their device in an alternative mode: they stopped the flow, allowing the gradient to diffuse laterally, and measured the bacterial distribution at the same channel cross-section over time (stopped-flow approaches are further discussed in the next section). The comparison showed that a 0.1–1 mm s^{-1} mean flow did not affect the chemotactic migration of *E. coli* HCB1. This is a valuable approach to isolating (or ruling out) the effect of flow on chemotaxis and, to the best of our knowledge, is the only microfluidic test of this kind.

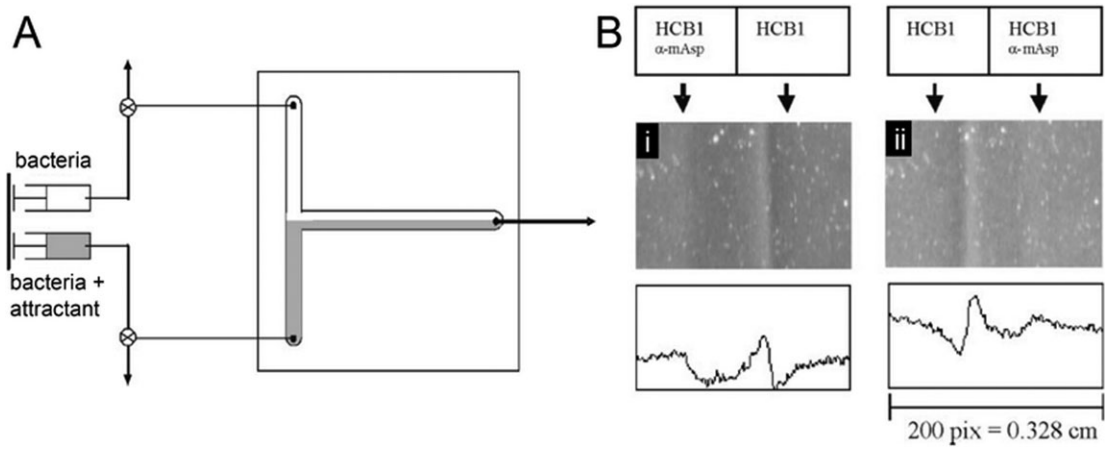

Fig. 3 The two-inlet parallel-flow device of Lanning *et al.*[73] (A) Two suspensions of *E. coli* HCB1 bacteria are injected into microchannels and converge as parallel flows (gray and white streams) within a single chemotaxis chamber. The concentration of bacteria in the two streams is the same, but one stream contains the chemoattractant α-methylaspartate. Diffusive mixing results in an attractant gradient across the chamber width (as in the device of Mao *et al.*;[70] Fig. 1). Lanning *et al.* demonstrated two modes of operation: (i) parallel-flow operation, where flow is maintained and bacterial concentrations are measured at different distances along the chamber; and (ii) stopped-flow operation, where bacterial concentrations are measured at one downstream location at different times after stopping the flow. (B) Transverse distribution of bacteria across the chamber, measured by light scattering. Grayscale intensities (top panels) are used to obtain relative cell concentrations (bottom panels). Bacterial bands migrating towards higher chemoeffector concentrations are visible. (Reproduced from ref. 73 with permission. Copyright 2008 John Wiley and Sons).

Application of this device further revealed the presence of dual migrating bands of *E. coli* in response to a 0.1 mM α-methylaspartate step gradient (but not for 0.01 mM). Double-band migration was reported previously,[74,75] but remains poorly understood. The hypothesis that dual bands result from two subpopulations of α-methylaspartate receptors, one with high and one with low affinity,[76] awaits further testing, and pursuing the chemical and molecular origins of these dual bands could represent a fruitful area of future research.

Porous two-inlet parallel-flow device

A closely related device was used by Long *et al.*[77] to study bacterial chemotaxis in an artificial subsurface environment. Circular cylinders of 200 μm diameter arranged in a hexagonal pattern, simulated soil with 40% porosity (Fig. 4A). The average velocity in the channel (5–20 m day^{-1}) was typical of groundwater flows. Gradients of α-methylaspartate were again formed across the channel width by two parallel streams, but *E. coli* HCB1 cells were only injected in the buffer stream. The bacterial distribution was obtained by counting cells within each pore (an interstice between cylinders) in ten adjacent fields of view (Fig. 4A). Similar to Lanning *et al.*,[73] the observed distribution was fitted numerically to the bacterial transport equation (modified for porous media) to quantify the Chemotactic Sensitivity Coefficient (see Table 1).

The observed chemotactic response (Fig. 4B) was larger than predicted, a fact that the authors attributed to within-pore dynamics. However, bacteria-surface interactions tend to hinder migration by hydrodynamic trapping,[78,79] suggesting that more work is needed to understand motility and chemotaxis in this complex environment, as recognized by the authors. Despite this, the study of Long *et al.*[77] highlights the versatility of microfluidic technology in including essential features of realistic environments while obtaining quantitative information on bacterial chemotaxis.

Microfluidic nutrient plume injector

Another example where a microfluidic gradient generator has been used to model a realistic bacterial microenvironment is the nutrient plume injector of Stocker *et al.*[13] This device mimics the plume of dissolved organic matter (DOM) trailing marine snow particles that settle in the ocean. The settling particle is represented as a 500 μm diameter polydimethylsiloxane (PDMS) cylinder, around which a DOM plume is created by means of a microinjector (Fig. 5A). Marine bacteria are injected *via* a second inlet and transported by the flow past the particle and plume, simulating particle settling (in the reference frame of the particle). Different settling speeds, and thus different plume shapes, are obtained by changing the flow rate (Fig. 5B).

Quantification of chemotaxis occurred by acquisition of movies at 51 locations along the plume, using computer-controlled motion of the microscope stage to cover 25 mm of the plume, and image analysis to automatically count individual cells. This is an example of the flexibility afforded by microfluidics in automating data acquisition, yielding large amounts of single-cell information with little increase in experimental effort.

The marine bacteria *Pseudoalteromonas haloplanktis* strongly accumulated by chemotaxis in the nutrient plume of slow particles (Fig. 5B), enhancing their exposure to nutrients by 400% relative to non-motile bacteria.[13] Because they occur ubiquitously in the ocean, these microscale responses could entail a significant acceleration in DOM turnover rates. Hence, despite the disparity in scales, microfluidics can shed light on the microscale mechanistic underpinnings of global-scale processes.

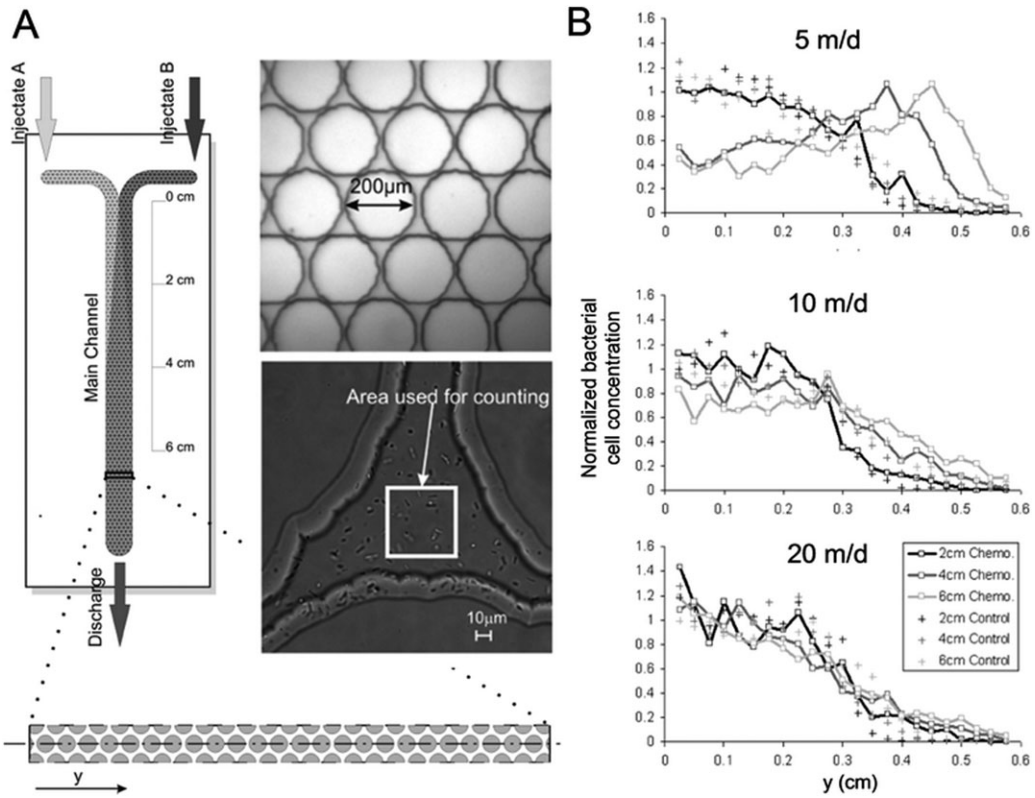

Fig. 4 **The porous parallel-flow device of Long *et al.*** [77] (A) A chemoeffector gradient between two parallel streams is formed by the same basic principle as the devices of Fig. 1 and 2. Injectate A contains a suspension of *E. coli* HCB1, while injectate B contains a solution of α-methylaspartate. The chamber mimics flow in a porous medium, represented as a collection of 200 μm PDMS cylinders (top micrograph). A 50 × 50 μm area within each pore (bottom micrograph) is used to count bacteria. (B) Transverse bacterial distribution for three positions along the chamber (2, 4 and 6 cm) and three mean flow speeds (5, 10 and 20 m day^{-1}). The concentration of α-methylaspartate increases from left to right. In the control experiments, injectate B was buffer without chemoeffector. (Reproduced from ref. 77 with permission. Copyright 2009 American Chemical Society).

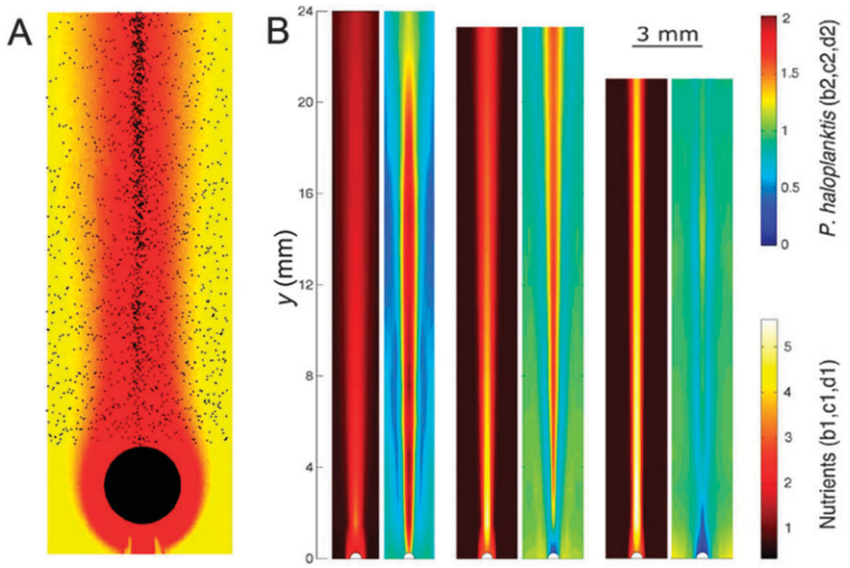

Fig. 5 **The nutrient plume injector by Stocker *et al.*** [13] (A) A 500 μm diameter PDMS cylinder models sinking marine particles that leak dissolved organic matter (DOM). A microinjector delivers the DOM that forms the plume (the tip of the microinjector is visible beneath the particle and the microinjector is further illustrated in Fig. 7). Flow in the microchannel, with mean speed of 110 μm s^{-1}, models realistic sinking rates in the ocean. Black dots show positions of individual *P. haloplanktis* bacteria, which strongly accumulated in the plume by chemotaxis. (B) The distribution of DOM ('nutrients') and *P. haloplanktis* in the wake of particles with three different settling speeds: 66, 220 and 660 μm s^{-1}. The particle is at $y = 0$. (Reproduced from ref. 13. Copyright 2008 National Academy of Sciences, USA).

µFlow device

Englert *et al.*[5] modified the three-inlet parallel-flow device[70] by adding a 'premixer gradient generator' upstream, in order to expose bacteria to a linear chemoeffector gradient (Fig. 6A). The premixer gradient generator[68] is a network of microchannels that can create an arbitrarily-shaped concentration profile by controlled diffusive mixing from two input streams. Thus, unlike the three-inlet parallel-flow device,[70] the µFlow device avoids exposing bacteria to a step-like chemoeffector profile. Furthermore, the initial, linear shape of the gradient is maintained for a larger distance along the channel (Fig. 6B), since diffusive equilibration is slower (gradients are weaker; Fig. 2B). This modification does not, however, fully solve the problem of creating a steady gradient, since the gradient ultimately still changes with distance downstream (*i.e.* with time).

Englert *et al.*[5] imaged *E. coli* RP437 cells 700 µm downstream from the bacterial injection point (Fig. 6C), amounting to a ~20 s exposure time of cells to the gradient, and quantified chemotaxis with the Chemotaxis Migration Coefficient (see Table 1). After performing tests with known attractants (0–100 µM L-aspartate) and repellents (0–225 µM $NiSO_4$), they studied *E. coli*'s response to gradients of cell-cell communication signals present in the human gastrointestinal environment: AI-2 (0–500µM), indole (0–500 µM), and mixtures of the two. Attraction to AI-2 was found to be greater than repulsion by indole, and the response to mixed gradients was biased towards AI-2. The authors concluded that AI-2 represents a preferential signal for the colonization of the gastrointestinal tract by enterohemorrhagic *E. coli*. These experiments provide a good example of the ability of microfluidics to create gradients of more than one chemoeffector simultaneously.

Although the µFlow device does not avoid the effect of fluid forces on bacteria, this flow could represent a realistic feature of the human gastrointestinal environment. If flows can in the future be matched to those of the gastrointestinal tract, this

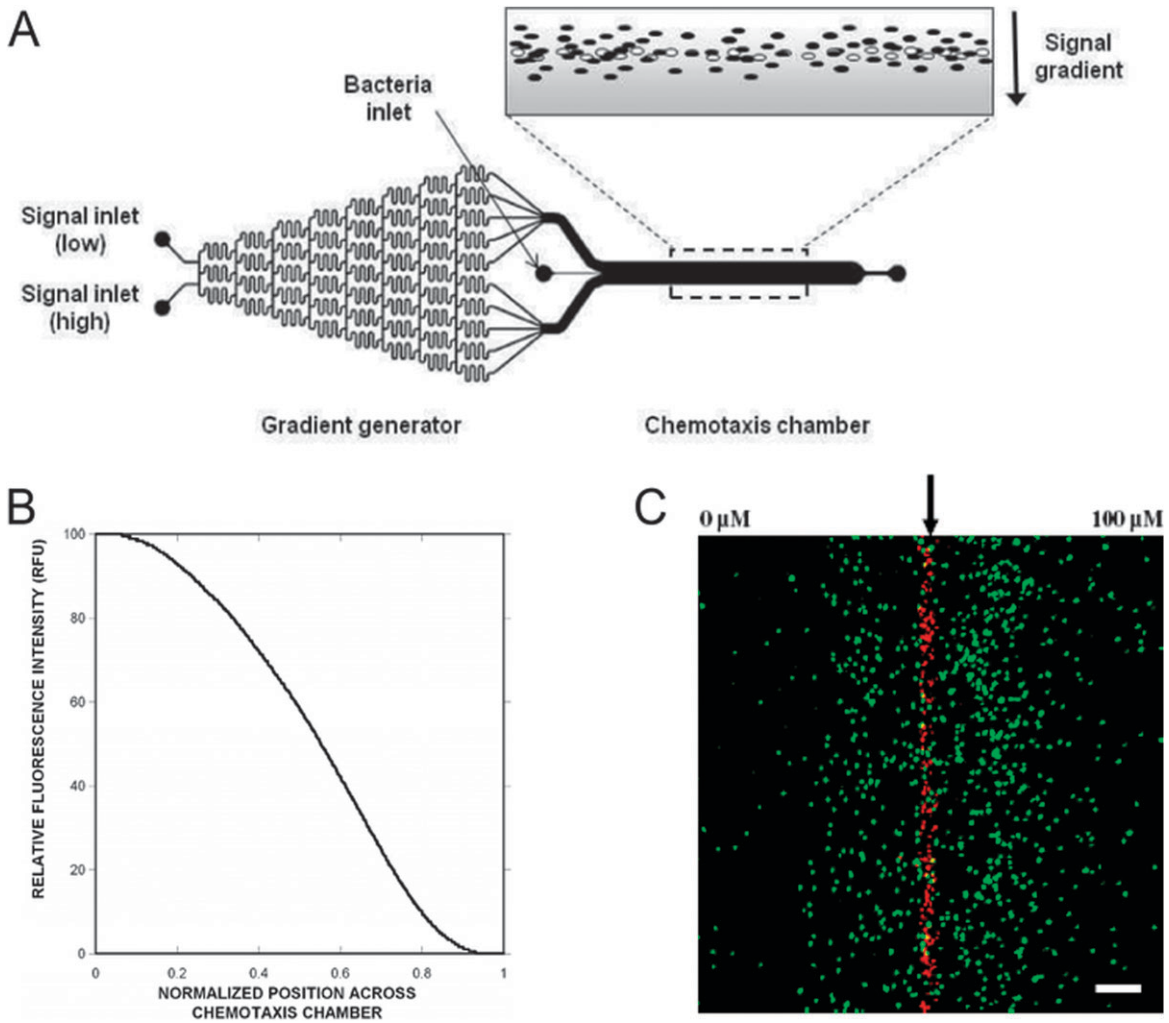

Fig. 6 **The µFlow device of Englert *et al.*[5]** (A) This device adds to the three-inlet parallel-flow device (ref. 58) an additional gradient generator that produces a nearly linear gradient of chemoeffector (panel B) upon entry into the chemotaxis chamber. Bacteria are injected along the axis of the chemotaxis chamber using a third inlet. (B) The concentration profile across the chemotaxis chamber 700 µm downstream of the injection point. (C) Epifluorescent image showing instantaneous positions of *E. coli* RP437 in a gradient of L-aspartate. Green and red dots represent live and dead bacteria, respectively. The spread of the live population is due to motility, while its drift towards the right is due to chemotaxis. The scale bar is 100 µm. (Reproduced from ref. 5 with permission. Copyright 2009 American Society for Microbiology).

will be a powerful approach to study the simultaneous action of chemical gradients and flow on chemotaxis of enterohemorrhagic bacteria.

Evaluation of flow-based gradient generators

Flow serves two purposes in flow-based gradient generators for bacteria chemotaxis: to set up gradients and to model environmentally realistic flows. When the goal is the latter, flow-based devices represent an excellent approach. Indeed, flow is nearly ubiquitous in the watery habitats of bacteria, and likely to be an important determinant of their motile behavior. In this respect, microfluidic gradient generators that operate under flow are a unique tool to capture the simultaneous effect of chemical cues and fluid mechanical forces on chemotaxis.

On the other hand, when one is interested in chemotaxis in the absence of flow, we suggest that alternative approaches that have recently become available (and are described below) are preferable. Observing chemotaxis in flowing conditions can introduce confounding factors that need to be controlled for in the best-case scenario, and can substantially alter outcomes in the worst case. The main effect of flow is to exert shear stresses on cells. In a wide rectangular channel of depth h, the shear stress at the top and bottom boundaries is $\tau_W = 6\mu Q/h^2$, where μ is the dynamic viscosity of the fluid and Q is the flow rate. Because microchannels are typically shallow, shear stresses can be large, as they increase inversely with the square of depth for a given flow rate. Hydrodynamic shear can reorient cells[80–82] and potentially impair chemotaxis,[83] making it difficult to distinguish between the active movement due to chemotaxis and the passive movement due to hydrodynamic shear. Slow flow rates mitigate the problem, but no-flow control experiments like those performed by Lanning *et al.*[73] are always desirable, if chemotaxis results are to be eventually compared among studies and the effects of chemical attraction and flow forces are to be teased apart.

A second drawback of flow-based configurations is that gradients are inherently unsteady (Fig. 2A and B). This unsteadiness results from the fact that the boundary conditions for the concentration profile, at the channel sidewalls, are no-flux boundary conditions. Steep initial gradients will change the fastest (Fig. 2A), because of the large diffusive flux, but even linear gradients will inexorably diffuse to homogeneity. In a flowing configuration, this temporal evolution amounts to an evolution with distance downstream. In some cases, one might be interested in explicitly including and accounting for this unsteadiness (some cases are described below). More often, however, this unsteadiness represents a constraint of the experimental design, limiting the time over which a bacterial population is exposed to the same gradient. Because the chemotactic response time is species-specific and one would ideally be able to extend observations over large times, this unsteadiness limits the range of applications of flow-based gradient generators. In particular, experiments with slow-swimming cells become prohibitive.[57]

A third disadvantage of flow-based devices is the difficulty of obtaining single-cell movement information. Chemotaxis can be investigated at two levels: the population scale and the single cell scale. In the former case, one quantifies bacterial distributions along a chemoeffector gradient and knowledge of bacterial positions is sufficient. In the latter case, one analyzes the swimming kinematics of single bacteria, often with the goal of obtaining a chemotactic velocity.[7] This second approach has its prime example in the classic three-dimensional tracking studies of *E. coli* performed by Howard Berg,[17] a hitherto unmatched feat of engineering in the field of bacterial motility and chemotaxis. Microfluidics enables both approaches,[7] but the single-cell approach requires absence of flow to be applied reliably. While one could potentially track single cells and subtract the flow velocity from the trajectories, this is often a noisy undertaking, particularly when flow speeds are comparable to or larger than swimming speeds.

These limitations can be overcome, to different degrees, by diffusion-based gradient generators, which create flow-free and shear-free environments for bacterial chemotaxis. These are described in the next section, focusing first on the generation of unsteady gradients, then on steady gradients.

6. Chemotaxis in flow-free, unsteady gradients

Bacterial chemotaxis can be studied in the absence of flow by producing gradients through purely diffusion-based techniques. While even flow-based gradient generators ultimately rely on diffusion to establish a gradient, the term 'diffusion-based' emphasizes that chemotaxis occurs and is observed in gradients that evolve only by diffusion, in the absence of flow. We begin by describing in this section 'stopped-flow' gradient generators, where flow is used to set up an initial gradient, but is then turned off, allowing the gradient to evolve by diffusion alone. These stopped-flow devices produce inherently unsteady gradients and are, in this respect, similar to the SFDC of Ford *et al.*[58] (which also uses stopped-flow) and to the classic capillary assay[50] (which relies on diffusion alone). In the next section, we describe techniques that eliminate not only the need for flow, but also the unsteadiness of the gradient.

Microfluidic nutrient pulse generator

In some environments, bacteria are prevalently exposed to inherently unsteady chemical cues. A prime example is aquatic ecosystems, chiefly the ocean, where bacteria experience pulses of dissolved organic matter, created by excretions by larger organisms or cell lysis events.[84,85] These result in localized injections of DOM that rapidly diffuse. Some of the constituents of this DOM can act as chemoeffectors for marine bacteria, which thus have a limited time to respond by chemotaxis. The scale of these releases is a fraction of a millimetre, suggesting that microfluidics is ideally suited for their study. Stocker *et al.*[13] introduced a method to replicate these ephemeral DOM pulses in a microfluidic device (Fig. 7), described in detail in Seymour *et al.*[86] The authors created a nutrient pulse by forming a band of chemoeffector along the axis of a microchannel by means of a 100 μm wide microfabricated injector (Fig. 7A and B). The width of the chemoeffector band is typically ~300 μm, but can be controlled by adjusting the

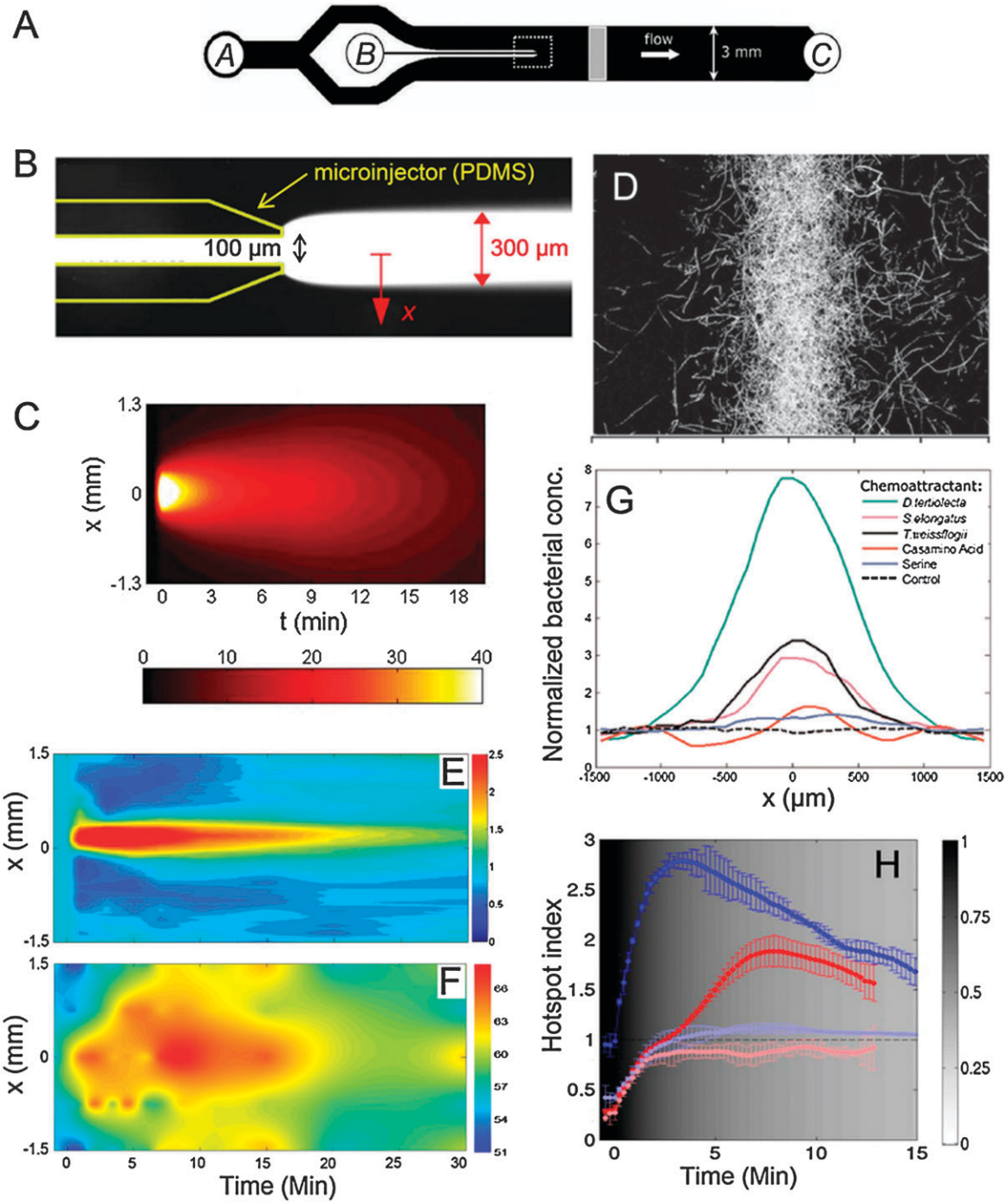

Fig. 7 **The nutrient pulse generator of Seymour *et al.*** [47] (A) The microchannel has two in-line inlets, one for a chemoeffector solution (inlet *A*) and one for a bacterial suspension (inlet *B*). Bacteria are transported by flow along the channel, where they are exposed to the band of chemoeffector created by the PDMS microinjector (magnified in panel B). The band width can be adjusted by changing the flow rates in inlets *A* and *B*. (C) Spatiotemporal evolution of the concentration field upon stopping the flow, compiled from epifluorescence microscopy of fluorescein concentration at 30 s intervals, showing the diffusion of the chemoeffector band across the channel. (D, E, F) Chemotaxis of the marine bacteria *Pseudoalteromonas haloplanktis* to a pulse of phytoplankton exudates. Strong and rapid chemotaxis is shown by accumulation of trajectories (D) and spatiotemporal accumulation plot (E). Tracking of individual bacteria showed a > 20% increase in speed of *P. haloplanktis* exposed to the phytoplankton exudates, as revealed by the spatiotemporal plot of swimming speed (F). (G) Transverse distribution of *P. haloplanktis* for various chemoeffectors. (H) Time evolution of the hotspot index (a measure of the accumulation in the chemoeffector band, see Table 1), showing that *P. haloplanktis* (blue curve) exhibits considerably stronger chemotaxis towards ephemeral pulses of phytoplankton exudates (blue) than *E. coli* HCB1 (red curve) does towards its most potent known chemoattractant (10 μM L-aspartate plus 10 μM L-serine). Light blue and light red curves represent control runs. The background colors are a measure of the mean attractant concentration in the central, 300 μm band. (Panels A, C, E, F: reproduced from ref. 47 with permission. Copyright © 2009 The University of Chicago Press. Panels B and H: reproduced from ref. 13 with permission. Copyright 2008 National Academy of Sciences, USA. Panels D, G: reproduced from ref. 86 with permission. Copyright 2008 American Society for Limnology and Oceanography).

relative flow rate in the two inlets.[86] Simultaneously, bacteria are flowed along the sides of the band, using a separate inlet.

The experiment starts by stopping the flow, simulating the release of the chemoeffector. At any given position along the channel, the chemoeffector band begins to diffuse laterally, mimicking a one-dimensional DOM pulse with a nearly Gaussian shape (Fig. 7C), to which bacteria respond by chemotaxis (Fig. 7D and E). To quantify bacterial chemotaxis, Seymour *et al.*[86] introduced a Chemotaxis Index (I_C; see Table 1), which describes the strength of bacterial accumulation within a given region, in this case the location of the chemoeffector band. The Hot Spot Index (H; see Table 1) of Stocker *et al.*[13] is similarly defined.

Stocker's group has applied this 'stopped-flow' approach to a range of chemotaxis studies on marine microbes. Stocker *et al.*[13] showed that the accumulation of *P. haloplanktis* in response to a nutrient pulse made of the exudates of the phytoplankton *Dunaliella tertiolecta* led to formation of bacterial hot spots within tens of seconds, and these accumulations persisted for $\sim$15 min (Fig. 7H). This response was $>$10 times faster than the response of the chemotaxis model organism *E. coli*, challenged with two of its most potent chemoattractants (10 μM L-serine and 10 μM L-aspartate). The marine bacteria achieved twice the nutrient exposure of *E. coli* HCB1, suggesting an adaptation to an environment made of small, ephemeral nutrient pulses. The higher swimming speed of *P. haloplanktis* (68 μm s^{-1}) compared to *E. coli* (31 μm s^{-1}) was important, but not sufficient to explain this superior capacity for patch exploitation, indicating that other aspects of the chemotaxis system of marine bacteria might be adapted to short-lived chemical cues. In a different study with the same device, Seymour *et al.*[47] tracked individual *P. haloplanktis* cells and found noticeable behavioral adaptations (*e.g.* increased swimming speed (Fig. 7F) and reduced turning frequencies inside the nutrient patch) contributing to persistent aggregation of cells. This work invites further research on the chemotaxis systems of *P. haloplanktis* in particular, and of marine bacteria in general.

A number of studies based on the nutrient pulse injector showed how pervasive chemotaxis is among marine microorganisms. Experiments with phytoplankton and protists, in addition to bacteria, showed a cascade of patch formation and exploitation and suggested that trophic interactions within the marine microbial food web might occur primarily within ephemeral resource patches.[47] Varying levels of chemotactic response were measured for three species of marine bacteria, *P. haloplanktis*, *Silicibacter* sp.(TM1040) and *Vibrio alginolyticus*, towards the exudates of the marine phytoplankton *D. tertiolecta* and *Thalassiosira weissflogii*[86] (Fig. 7G) and of two species of marine cyanobacteria, *Synechococcus elongatus* and *Prochlorococcus marinus*.[48] These behavioral responses of marine bacteria to phytoplankton exudates are likely to be an important component of phytoplankton-bacteria interactions, thus affecting bacterial growth and carbon turnover rates in the ocean.[48,86] This response becomes intriguing when it is directed towards (otherwise) toxic phytoplankton. Using the pulse microinjector, Seymour *et al.*[46] found that the chemical products of the toxic species *Heterosigma akashiwo* attract the marine bacteria *V. alginolyticus* and *Silicibacter sp.*, a coupling that may have important consequences on the growth and toxicity of phytoplankton species that form harmful algal blooms.[46]

Most recently, Seymour *et al.*[12] demonstrated that the marine bacteria *Silicibacter* sp. (TM1040) and *P. haloplanktis*, among several other marine microorganisms, exhibit positive chemotaxis towards dimethylsulfoniopropionate (DMSP). DMSP is a phytoplankton-produced compound whose breakdown products include dimethylsulfide (DMS), a volatile compound that favors cloud formation in the atmosphere. *P. haloplanktis* showed a very strong response towards high concentrations (500 μM) of DMSP, with chemotactic velocities reaching up to 44% of their mean swimming speed, resulting in an increased exposure to DMSP of up to 66%. This response of marine bacteria can have far-reaching effects on the sulfur cycle, as it alters the balance of the chemical transformations of DMSP. This series of studies further demonstrates the ability of microfluidics to model essential features of the chemical landscape of natural microbial environments, while enabling a quantitative characterization of the cells' response.

Linear gradient generator with hydrodynamic focusing

Another example of the 'stopped-flow' type microfluidic assay, where unsteady gradients are created by diffusion, is the linear gradient generator of Jeon *et al.*[87] (Fig. 8A) The fundamental operation is similar to the microfluidic nutrient pulse generator, but the initial gradient is linear instead of peaked. The flow in the main channel results from the confluence of flows from three microchannels (Fig. 8A and B). One of the outer channels delivers a thin bacterial suspension, generated by means of a hydrodynamic focusing technique where an outer sheet of fluid compresses the bacterial stream to nearly a single row of bacteria. This ensures a small number of bacteria in any field of view (1–5 cells in the field of view using a 10× objective), facilitating cell tracking. The other two channels are connected to a network of microchannels that mixes chemoeffector and buffer to form a linear gradient upon entry in the main channel (Fig. 8C), through a principle similar to the 'premixer gradient generator'[68] described above.

After stopping the flow, Jeon *et al.*[87] tracked the response of individual *E. coli* RP437 cells towards L-aspartate and quantified chemotaxis by means of a single-cell based Migration Index (see Table 1). A 0.22 mM mm^{-1} gradient was found to elicit the strongest chemotactic response (Fig. 8D). Steeper gradients elicited weaker responses, likely due to receptor saturation. Through direct measurements, the authors showed that the magnitude of the gradient decreased by 20% over the first 30 s, when data were acquired, and by 45% over the first 60 s. Although the gradient generated by this device is in general unsteady, as in all stopped-flow assays, acquisition times much shorter than the diffusional equilibration time of the concentration profile (Fig. 2A and B) reduce the temporal variability of the gradient to which bacteria are exposed.

Microfluidic capillary

A different design to generate unsteady, diffusion-driven gradients was used by Ahmed and Stocker[7] to connect

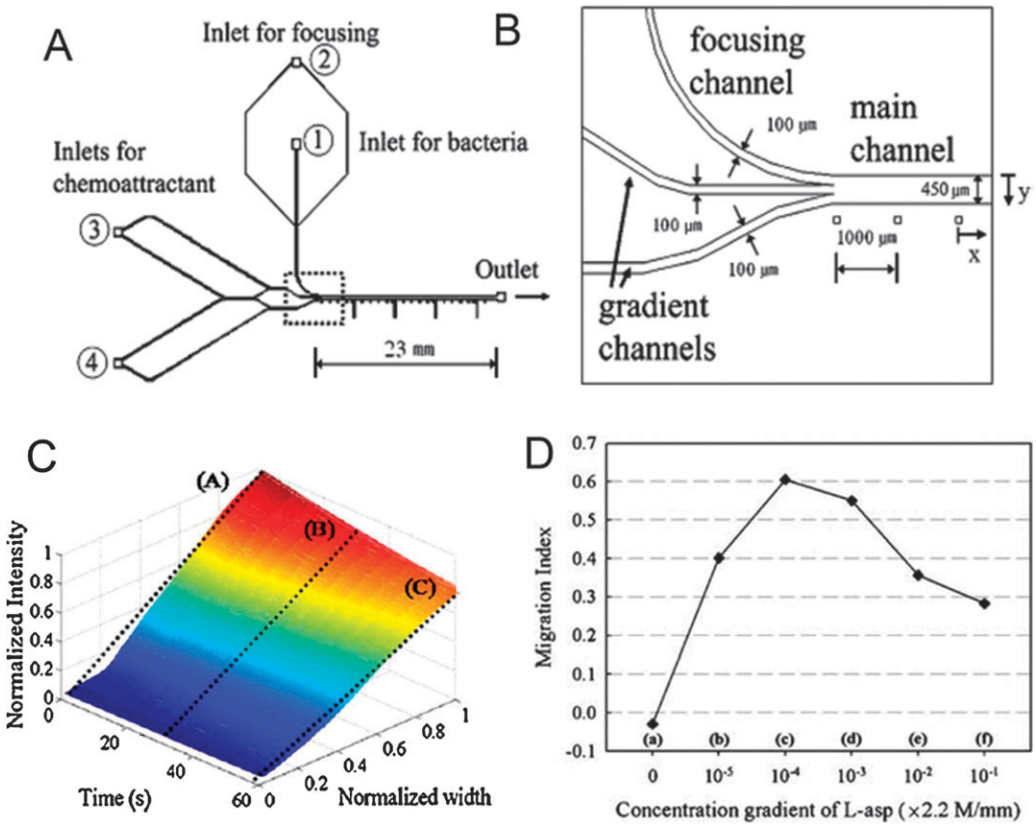

Fig. 8 The linear gradient generator with hydrodynamic focusing of Jeon *et al.*[87] (A) Two 'gradient channels' (see magnified view in B) deliver a chemoeffector gradient generated upstream to the main channel, which serves as the chemotaxis chamber. The gradient generator operates by splitting and mixing streams with different concentrations. A 'focusing channel' injects a stream of bacteria on one side. The bacterial stream is maintained very thin by buffer injection on either side, *via* inlet 2, to limit the number of cells in the field of view and facilitate tracking. (C) Measured evolution of the concentration profile 2 mm downstream of the junction, after stopping the flow. (D) The strongest observed chemotaxis of *E. coli* RP437 towards L-aspartate occurred for a 0.22 mM mm^{-1} gradient, as measured by the Migration Index (see Table 1). (With kind permission from Springer Science + Business Media: ref. 87, Fig. 1, 4 and 7).

microscale and macroscale descriptions of chemotaxis. *E. coli* AW405 (also known as HCB1) cells were exposed to gradients of the chemoattractant α-methylaspartate generated in a 0.6 mm wide microchannel (the 'microcapillary') attached perpendicularly to a second, larger microchannel (Fig. 9A and B). This device was inspired by the classic capillary assay[50] and by a related millifluidic version,[52] though with the important additional ability to directly count and track bacteria within the microcapillary.

The microcapillary was initially uniformly filled with a solution of chemoattractant (Fig. 9C). Flow containing buffer solution (no chemoattractant) was initially applied in the main channel, with the purpose of creating a zero-concentration boundary condition for the chemoattractant at the mouth of the microcapillary. When a gradient of chemoattractant was formed by diffusion (Fig. 9D), the flow in the main channel was switched to buffer containing a bacterial suspension. A fraction of the bacteria from the main flow swam into the microcapillary (Fig. 9B) and their trajectories were recorded by videomicroscopy at different positions along the microcapillary (Fig. 9E and F) and different times. Because of the small width of the microcapillary, fluid within it remained quiescent. Chemoattractant diffused from the microcapillary into the main channel, creating a concentration profile within the capillary with a broad range of local gradients and concentrations. This was exploited to acquire data on the bacterial response to multiple concentrations and gradients within a single experiment, by computer-controlled motion of the microscope stage and automated data acquisition.

Chemotactic velocities (see Table 1) were calculated by extracting the average run times up and down the gradient, respectively, from multiple individual cell trajectories in each field of view (Fig. 9G and H). By exploring a wide range of concentration conditions (Fig. 9J), Ahmed and Stocker[7] observed chemotactic velocities as high as 35% of the swimming speed (Fig. 9I), considerably larger than typical literature values (6–23%[17,75,88]). The magnitude of the chemotactic velocity decreased in regions where chemoattractant concentrations were higher than 0.125 mM, consistent with a reported receptor-ligand dissociation constant K_D of 0.125 mM.[89] The novelty of this approach consisted in extracting population-scale information from single-cell observations, taking advantage of the flexibility of microfluidics to generate controlled conditions while observing single cells. This enabled the testing of a population-scale model[59] of the dependence of chemotactic

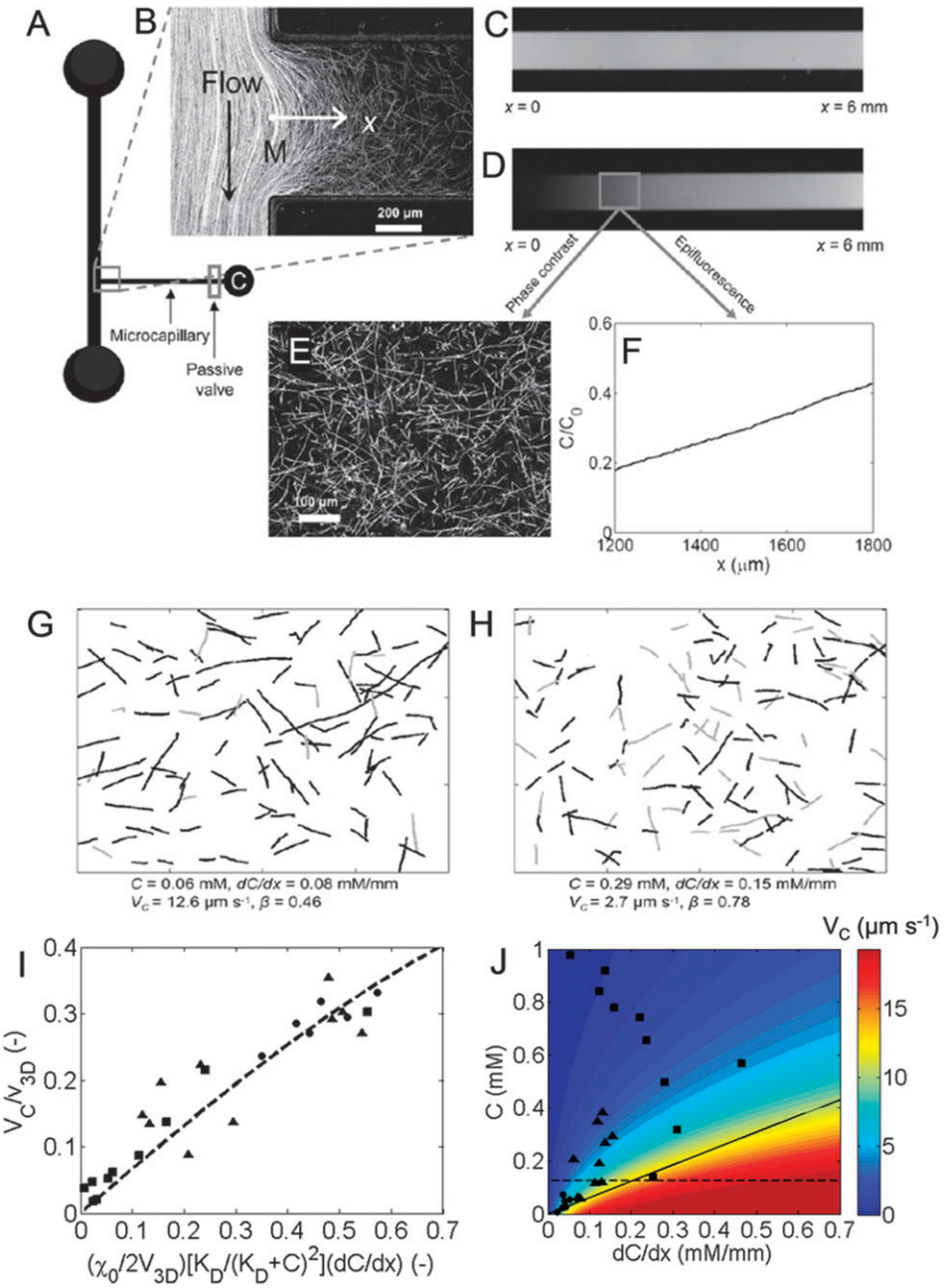

Fig. 9 **The microfluidic capillary assay of Ahmed *et al.*** [7] (A) The 'microcapillary' is a 600 μm wide microchannel with one end open to a wider reservoir channel flowing a suspension of *E. coli* HCB1 cells. (B) A fraction of the cells from the reservoir flow can swim into the microcapillary. (C) A solution containing the attractant α-methylaspartate and the tracer fluorescein is injected into the microcapillary *via* inlet c (panel A) and has an initially uniform concentration, as confirmed by imaging tracer fluorescence. (D) The concentration field subsequently evolves by diffusion into the main channel. (E) Cell trajectories are recorded at different locations and times along the microcapillary, together with the tracer concentration profile (panel F). (G, H) Bacterial trajectories recorded for two different concentrations and gradients (C and dC/dx), showing cells swimming up (black) and down (grey) the gradient. Trajectories yield the chemotactic velocity, V_C (see Table 1). Strong chemotaxis is visible in G, where most cells swim up the gradient (high V_C), but not in H (low V_C), likely due to receptor saturation. (I) Observed values of the chemotactic velocity V_C relative to the 3D swimming speed, v_{3D}, for *E. coli* HCB1 exposed to α-methylaspartate gradients. K_D is the receptor-ligand dissociation constant (=0.125 mM, ref. 80) and χ_0 is the Chemotaxis Sensitivity Coefficient (see Table 1). (J) V_C as a function of C and dC/dx from a theoretical model[47] (background colors), showing the wide range of conditions tested with the microfluidic device. The dashed line indicates $C = K_D$. Symbols in (I, J) represent experiments with different initial α-methylaspartate concentrations in the microcapillary (■: 1 mM, ▲: 0.5 mM, ●: 0.1 mM). (Reproduced from ref. 7 with permission. Copyright 2008 Elsevier).

velocity on chemoeffector concentration and concentration gradient (Fig. 9I), and the quantification of the Chemotactic Sensitivity Coefficient (see Table 1) of *E. coli* towards α-methylaspartate.

Evaluation of diffusion-based, unsteady gradient generators

The unsteadiness of gradients generated by stopped-flow assays can be used to one's advantage in two ways. First, unsteadiness

might represent a real feature of an environmental signal, as in the nutrient pulses often experienced by marine bacteria.[13,85] In this case, microfluidics provides a powerful approach to mimic the microenvironment of a bacterial population, because of the ability to create ephemeral gradients at the appropriate spatial and temporal scales. Coupled with videomicroscopy, this approach enables the observation of the bacterial response with high spatial and temporal resolution. For example, Stocker *et al.*[13] acquired data on the bacterial distribution every 13 s, for several minutes (Fig. 7H). Second, the unsteadiness can be exploited to characterize bacterial responses to a wide range of concentrations and concentration gradients within a single experiment, as demonstrated by Ahmed and Stocker.[7]

Unsteadiness is not always an advantage, but some unsteady gradient generators can be of use even when one is interested in the response to steady gradients. When the stopped-flow assay is operated on short timescales, the gradient is steady to a good approximation (*e.g.* Jeon *et al.*[87]). This approach is especially useful for quantifying chemotaxis when the timescale of gradient relaxation (Fig. 2B) is much greater than the characteristic times of sensing and behavioral processes. However, for more versatile studies in time-invariant concentration profiles, the steady gradient generators described in the following section are of particular interest. These devices eliminate nearly all practical constraints on observation times, and thus can be applied to slow responses including sensory adaptation and population migrations over long length scales.

7. Chemotaxis in flow-free, steady gradients

The incorporation of porous materials such as hydrogels and porous membranes within microfluidic devices has enabled a quiet, yet nevertheless significant revolution that might be fairly described as a breakthrough for bacterial chemotaxis studies: the creation of steady chemical gradients in an environment free of flow or shear. The general operational principle is to observe bacteria within a microfluidic chamber (the 'test channel') that is coupled through hydrogel layers to two flanking chemoeffector reservoirs. The hydrogel permits the passage of molecules by diffusion, but completely blocks advection. By maintaining constant concentrations in the reservoirs, one can create a flow-free environment in the test channel with constant-concentration boundary conditions. In contrast to the *no-flux* boundary conditions of flow-based devices, *constant-concentration* boundary conditions result in a steady concentration profile, determined by the reservoir concentrations. Once established, this concentration profile remains invariant and can in principle be preserved indefinitely, as long as the reservoirs are maintained at constant chemoeffector concentration. This can be easily achieved by replenishing the reservoirs either periodically or by continuous flow. This approach considerably extends the range of timescales over which chemotaxis experiments can be carried out and enables chemotaxis studies with truly constant concentration profiles. Below we describe different configurations that implement this principle.

Nitrocellulose-based linear gradient generator

The first example of a steady gradient generator for bacterial chemotaxis was the device created by Diao *et al.*[90] A nitrocellulose membrane, from which three parallel channels were carved out with a CO_2 laser, was sandwiched between a glass slide and a plexiglass clamping manifold, to provide adequate seal (Fig. 10A and B). One of the outer channels ('source channel') contained a solution of chemoeffector in buffer, the other ('sink channel') contained buffer only. Here, and in the description of related devices in subsequent sections, we refer to these source and sink channels as 'feeder channels'. In general,

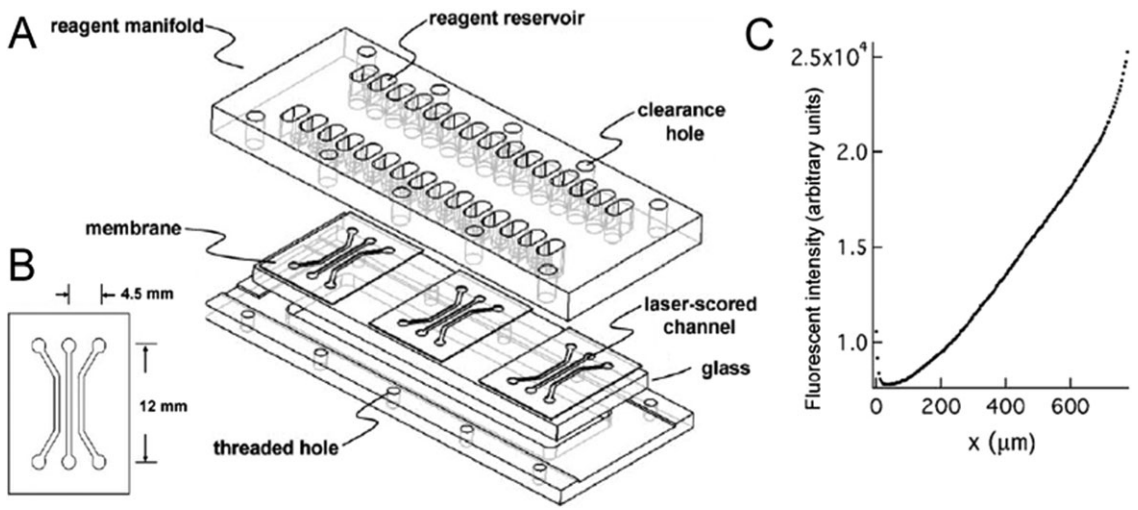

Fig. 10 The nitrocellulose-based linear gradient generator of Diao *et al.*[90] (A) Three channels are laser-scored from a nitrocellulose membrane (see detail in B). The outer two channels are the feeder channels (or 'reservoirs'), the central one is the test channel. Three such devices are shown in the schematic in A. The membrane lies between a glass slide and a clamping device. The two reservoirs contain a chemoeffector solution and buffer, respectively, and can be replenished through holes in the clamping device. Diffusion between the two reservoirs creates a concentration gradient within the nitrocellulose membrane. That gradient also spans the test channel. (C) The steady concentration profile in the test channel is almost linear. (Reproduced from ref. 90 with permission. Copyright 2005 The Royal Society of Chemistry).

we can denote the chemoeffector concentrations as C_0 in the source channel and C_1 in the sink channel ($C_1 = 0$ in Diao *et al.*[90]). Diao *et al.*[90] maintained C_0 and C_1 nearly constant by manually replenishing the reservoirs that provided gravity-induced flow through the feeder channels.

Diffusion of chemoeffector molecules from the source to the sink channel establishes a gradient of chemoeffector within the nitrocellulose membrane, in the direction perpendicular to the feeder channels. This gradient forms over a timescale $T \sim L^2/D$, where L is the distance between the feeder channels

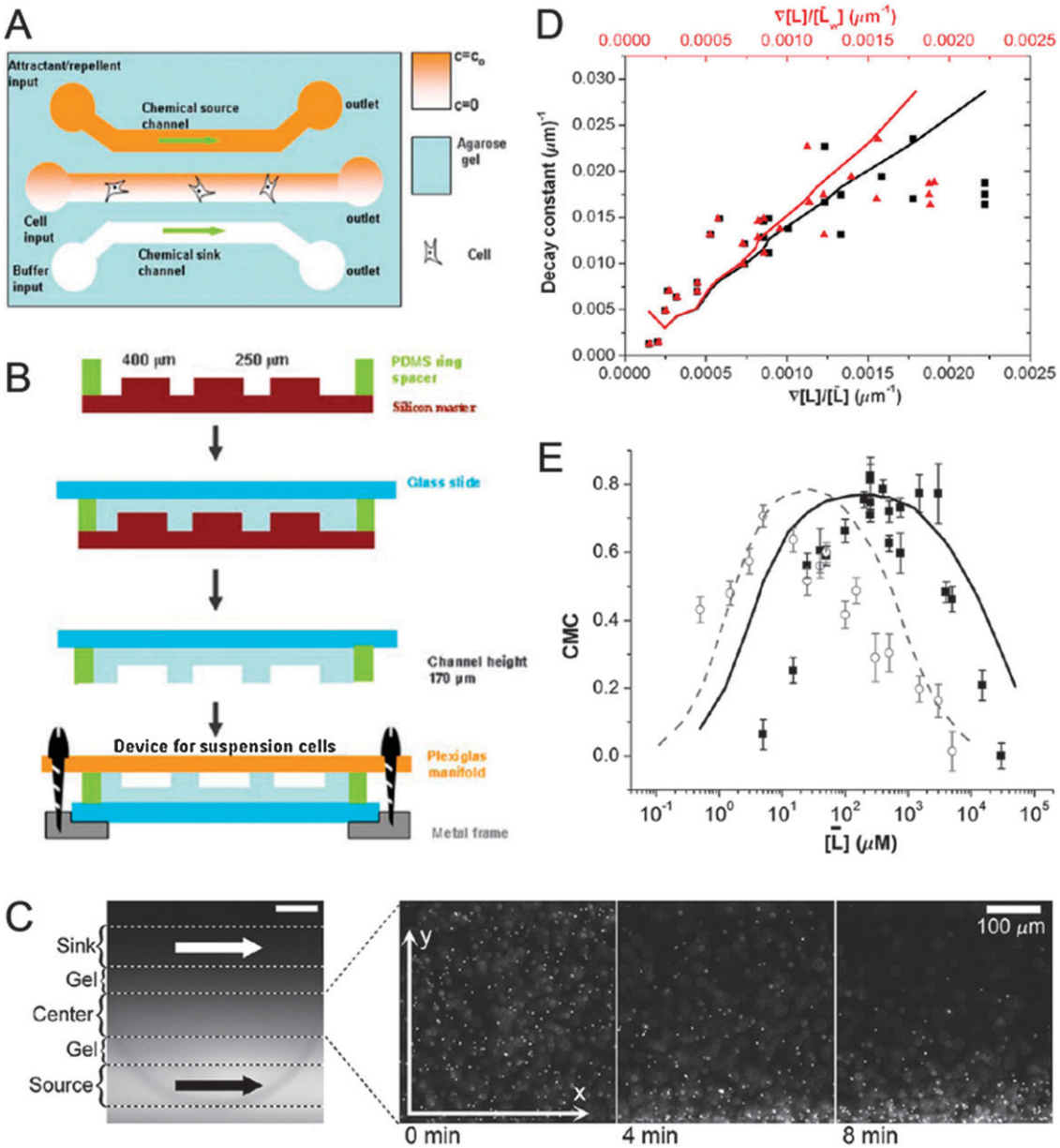

Fig. 11 **The agarose-based linear gradient generator of Cheng *et al.*[91]** (A) The three-channel design is similar to that of the device in Fig. 10. Two feeder channels (source and sink channels) are used to establish a gradient in the underlying agarose layer. Cells are injected in a central test channel. (B) Schematic of the fabrication technique and device assembly. (C) Epifluorescence micrographs showing the chemoattractant concentration field, visualized with fluorescein (left panel), and the distribution of *E. coli* RP437 at various times after injection of the cells and chemoeffector (right panels). (D) The spatial decay constant (obtained by fits to the nearly exponential steady-state bacterial distribution profile) as a function of the relative chemoeffector gradient, $\nabla[L]/[L]$ ($= \nabla(\log[L])$, where [L] is the chemoeffector concentration. The monotonic increase confirmed that *E. coli* uses logarithmic sensing for chemotaxis. The spatial decay constant was interpreted as the ratio of the chemotactic velocity to the random motility coefficient. (E) The Chemotactic Migration Coefficient (CMC, see Table 1) as a function of the mean chemoeffector concentration, for a constant value of $\nabla[L]/[L]$. A strong chemotactic response ($CMC \geq \frac{1}{2}CMC_{MAX}$) was observed over three orders of magnitude in mean concentration for both α-methylaspartate (10 μM–10 mM) [■] and L-serine (1 μM–1 mM) [○]. Lines in (D, E) represent theoretical results. (Panels A and B: reproduced from ref. 91 with permission. Copyright 2007 The Royal Society of Chemistry. Panel C, D, E: reproduced from ref. 92 with permission. Copyright 2009 Elsevier).

(measured between the two edges closest to each other) and D is the diffusivity of the chemoeffector through the nitrocellulose membrane (Fig. 2C and D). Diao *et al.*[90] reported a time of ~20 min to achieve a steady gradient (shown in Fig. 10C), consistent (though somewhat less) than the diffusive timescale predicted using $L = 0.8$ mm and $D = 10^{-10}$ m^2 s^{-1} (~2 h). The middle channel ('test channel') is filled with a suspension of bacteria. Because the test channel lies between the feeder channels, it experiences the same gradient of chemoeffector established within the nitrocellulose membrane.

Diao *et al.*[90] obtained the bacterial distribution across the width of the test channel by labeling bacteria with GFP and imaging by epifluorescence microscopy. The Chemotactic Migration Coefficient (see Table 1) was then used to quantify the strength of chemotaxis. Test experiments showed that *E. coli* RP437 exhibited positive chemotaxis in L-aspartate gradients ranging from 0.001 to 1 mM mm^{-1} and negative chemotaxis in a 0.1 mM mm^{-1} glycerol gradient. The intensity of the response towards L-aspartate increased with the magnitude of the gradient up to 0.1 mM mm^{-1}, beyond which it decreased, likely due to receptor saturation. Further experiments with quorum sensing mutants showed that the ability of *E. coli* RP437 to produce or sense the quorum sensing signal molecule AI-2 has no bearing on their chemotactic response.

This study provided the fundamental idea and ground work for subsequent developments in diffusion-based devices for bacterial chemotaxis. There were, however, two main limitations in this first-generation device. The first relates to fabrication and assembly of the device, which could not prevent residual flow for test chambers thicker than 140 μm. Residual flow is particularly detrimental in these experiments, since it disrupts the chemoeffector gradient as well as the ability to accurately track cells. The second limitation relates to the relative timing of the gradient setup and cell injection. Because the test channel is embedded in the membrane, the gradient in the test channel forms by horizontal diffusion, starting from the time of injection of the cells. This requires significant time (several minutes), during which the cells in the test channel are exposed to transient gradients. Subsequent studies by this group and others have exploited the advantages of soft lithography and rapid prototyping techniques to overcome these limitations and simplify fabrication. These are described in what follows.

Agarose-based linear gradient generator

Cheng *et al.*[91] replaced the nitrocellulose membrane with agarose (a hydrogel), where the two feeder channels and the test channel were patterned (Fig. 11A and B). This modification has a number of advantages: (i) if properly sealed, this device can completely eliminate residual transverse flow within the test channel; (ii) agarose can be easily and accurately molded using rapid prototyping techniques (Fig. 11B); (iii) diffusion in agarose occurs at rates that are very close to those in water; and (iv) agarose is highly transparent, when a thin layer of intermediate agarose content is used (*e.g.* a 1 mm thick layer with 3% weight/volume agarose), enabling visualization of cells by microscopy through the agarose layer (Fig. 11C).

Kalinin *et al.*[92] quantified the steady-state distribution of *E. coli* RP437 along linear chemoeffector gradients of magnitude ∇[L], and found this bacterial distribution to be well fit by an exponential function. The spatial decay constant of this fitted profile, which characterizes the strength of accumulation, was found to increase monotonically with the relative chemoeffector gradient, ∇[L]/[L] (Fig. 11D). The latter can also be written ∇(log[L]), implying that *E. coli* senses the gradient of the logarithmic chemoeffector concentration. This is the first population-scale experimental demonstration of *E. coli*'s 'logarithmic gradient sensing property', which had been predicted theoretically,[29] based on prior experimental results.[27,93]

Through experiments over a wide range of chemoeffector concentrations, [L], performed by keeping the relative gradient ∇[L])/[L] constant, Kalinin *et al.*[92] further found that the sensitivity peak of *E. coli* RP437 to α-methylaspartate (as characterized by the Chemotaxis Migration Coefficient, or CMC; see Table 1) spans a broad concentration range, from 25 μM to 3 mM (Fig. 11E). These findings are in agreement with recent theoretical results using a two-state model for receptor activation, in which the active and inactive receptor states bind ligand with different affinities.[94] Kalinin and coworker's results are an excellent demonstration of how microfluidics can be brought to bear on important open questions in bacterial chemotaxis.

In a second set of experiments with the same device, Kalinin *et al.*[95] showed that opposing gradients can be formed by injecting two different chemoeffectors, one in each feeder channel (Fig. 12A and B). They exposed *E. coli* to competing gradients of its two most potent known chemoattractants, L-serine (sensed by the Tsr receptor) and α-methylaspartate (sensed by the Tar receptor) (Fig. 12C) and found that their chemotactic preference (quantified using CMC; see Table 1) depended on the Tar/Tsr expression-level ratio (Fig. 12D). The latter, in turn, varied with growth conditions, as determined by quantitative immunoblot measurements, with preference for serine (α-methylaspartate) at lower (higher) values of OD_{600} (Fig. 12C). These studies provide an excellent demonstration of the potential of microfluidics in yielding novel insights on bacterial chemotaxis systems, stemming from accurate control over chemical environments and the ability to obtain high quality data on the chemotaxis response.

Agarose-PDMS based linear gradient generator

Ahmed *et al.*[96] have characterized in detail the concentration fields established within agarose-PDMS-based gradient generators, comparing three alternative designs to generate steady gradients. The planar layout, with a test channel between two feeder channels, is analogous to that used by Diao *et al.*[90] and Cheng *et al.*,[91] but different configurations were explored in terms of the vertical arrangement of the channels. Furthermore, continuous-flow feeder channels, rather than open source-sink reservoirs used before,[97,98] bypassed the need for periodic manual reservoir replenishment.

The modified design uses a 1 mm thick agarose layer sandwiched between a PDMS layer (above) and a glass slide (underneath) (Fig. 13A–C). Clamping manifolds, used by

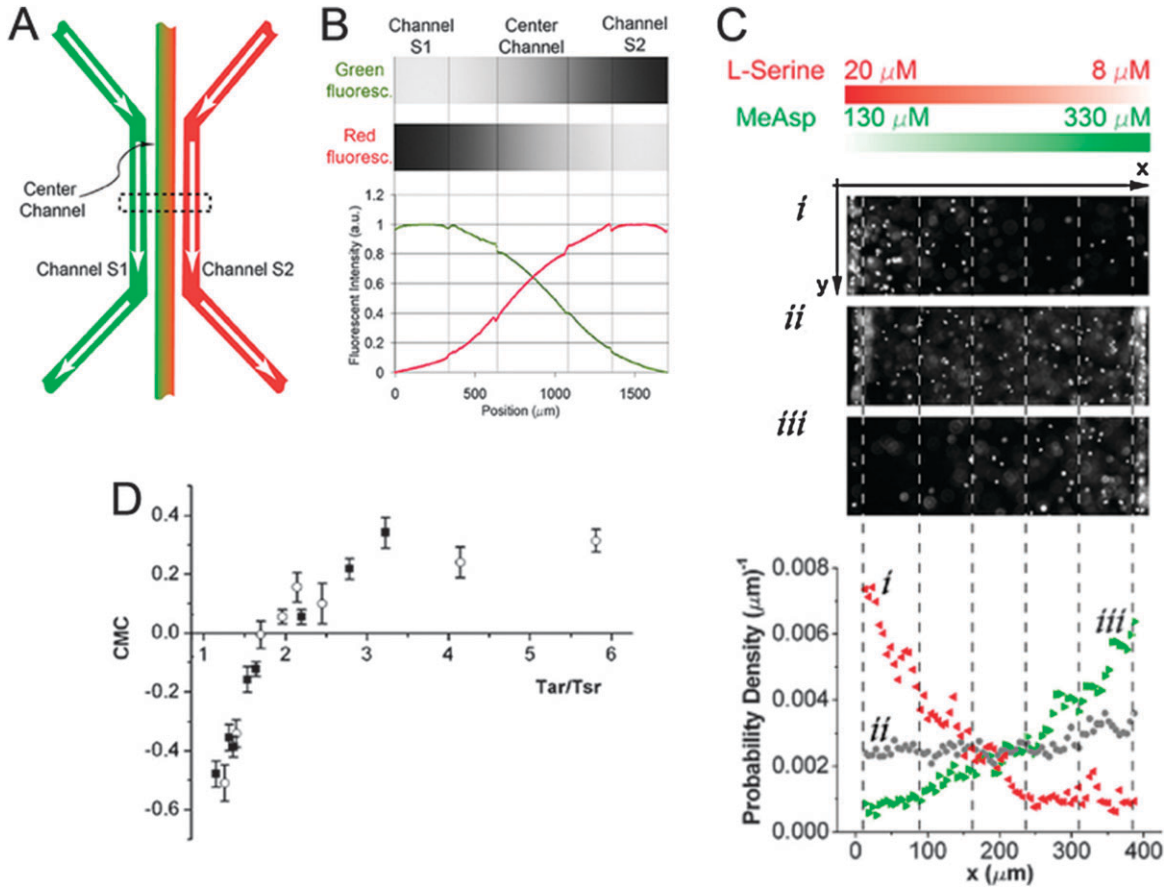

Fig. 12 The agarose-based linear gradient generator of Cheng *et al.*[91] applied to produce two opposing gradients. (A, B) Opposing gradients are generated by injecting a different chemical in each of the two feeder channels (here, green fluorescein and red rhodamine). (C) Response of *E. coli* RP437 to opposing gradients of L-serine and α-methylaspartate (MeAsp). *E. coli's* preference changes with its growth stage (cases i, ii, iii show the responses of *E.coli* harvested at OD_{600} of 0.26, 0.53 and 0.65 respectively). (D) Chemotactic Migration Coefficient (CMC; see Table 1) of *E. coli* RP437 exposed to opposing gradients of L-serine and α-methylaspartate as a function of the Tar/Tsr receptor ratio. Positive (negative) CMC values indicate a preference for α-methylaspartate (L-serine). Panels (C, D) demonstrate the link between substrate preference and expression of different receptors at different stages of growth. Symbols refer to culture conditions with different dilution ratios. (Panels A, B, C, D: reproduced from ref. 95 with permission. Copyright 2010 American Society for Microbiology).

Cheng *et al.*[91] to guarantee a seal and prevent leakage, were also omitted to simplify the design and operation. An effective seal between the agarose and PDMS layers was achieved by driving flow in the feeder channels by negative, rather than positive pressure.

Gradients in the test channel were quantified by confocal laser scanning microscopy (CLSM), as the authors found that wide-field fluorescence measurements of the test-channel concentration profile were corrupted by out-of-focus fluorescence from the underlying agarose layer. The latter findings throw light on the potential pitfalls of gradient characterization by fluorescence in devices of this type, including those used in the studies of Cheng *et al.*[91] and Kalinin *et al.*[92,95]

Three different designs were analyzed for their gradient generation performance. In design 1, all three channels are patterned in the PDMS layer (Fig. 13A). In design 2, they are patterned in the agarose layer (Fig. 13B). In design 3, the feeder channels were patterned in agarose and the test channel in PDMS (Fig. 13C). CLSM, in conjunction with the injection of 0.1 mM fluorescein in the source channel, showed that the steady-state gradient in the test channel, though linear, was 24–57% (depending on the design) weaker in magnitude than the gradient expected based on a linear decrease of concentration between the feeder channels (Fig. 13D). The latter represents the solution to the one-dimensional diffusion problem and has been assumed in previous studies.[90,91] The discrepancy is due to the two-dimensional nature of diffusion in these devices, in which the source and sink channels do not penetrate the entire depth of the agarose layer. This was confirmed by numerical simulations of the full two-dimensional diffusion problem, which predict a nonlinearity in the concentration profiles within the hydrogel regions closest to the feeder channels, with a consequent reduction in the gradient magnitude within the test channel (Fig. 13E). These findings suggest that studies requiring accurate quantification of chemoeffector gradients need to take into account the precise geometry of the gradient generator.

Design 3 was selected as the optimal one for bacterial chemotaxis experiments, as it combines operational flexibility (ability to fabricate more complex test-channel layouts) and minimal discrepancy between the expected and observed gradient. The performance of this device was then characterized directly in

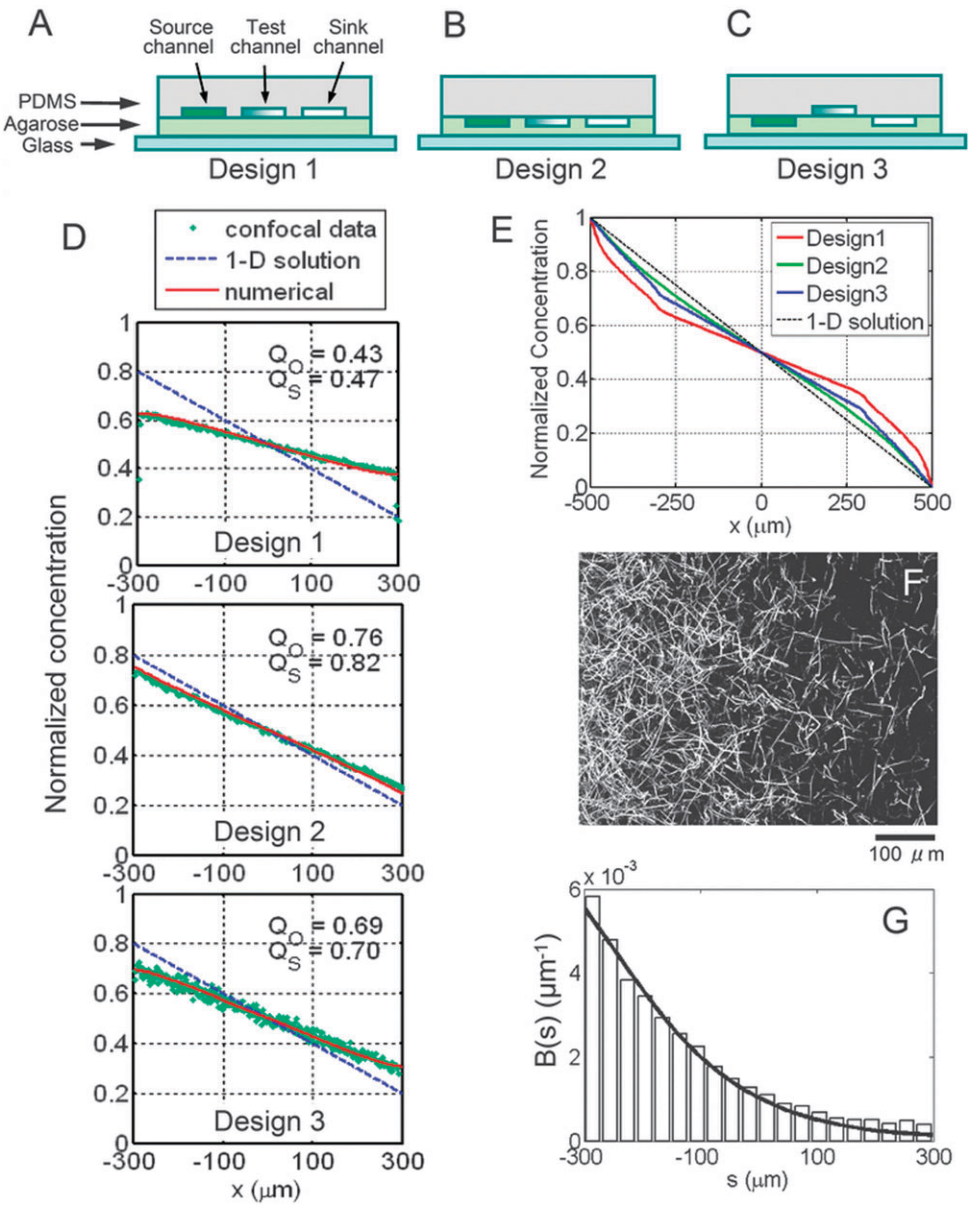

Fig. 13 The agarose-PDMS based linear gradient generator of Ahmed *et al.*[96] (A, B, C) Schematic vertical cross-sections of three different designs of the diffusion-based gradient generator to create steady, linear gradients. The edge-to-edge distance between the feeder channels was L = 1 mm. Design 2 is equivalent to the design of Cheng *et al.*[91] Ahmed *et al.* showed that by setting $H \ll H_A$, where H and H_A are heights of the test channel and agarose layers, respectively, this class of diffusion-based devices can establish the test-channel gradient very rapidly ($\sim$10 s for typical values of H = 50 μm and H_A = 1 mm). (D) Confocal laser scanning microscopy measurements of the tracer fluorescein (green dots), confirmed by numerical simulations (red curve) revealed that the concentration profile is very close to linear across the 600 μm wide test channel, but the gradient is shallower than predicted by the one-dimensional diffusion equation (blue dashed line). The difference is design-dependent, as shown by Q_O (Q_S), which measures the ratio of the observed (numerically predicted) gradient, relative to the 1D gradient. (E) Numerical simulations showed that, when measured across the entire distance between the feeder channels, the concentration profile is nonlinear, which explains the lower magnitude of the gradient in the test channel compared to the 1D prediction. (F) Trajectories of *E. coli* AW405 (also known as HCB1) exposed to a linear, 0.1 mM mm^{-1} gradient of α-methylaspartate (towards the left), using Design 3. The chemotactic response is evident in these data obtained by motion analysis of phase-contrast images. (G) Normalized distribution of *E. coli* cells along the gradient, $B(s)$, from experiments (bars) and a numerical simulation (curve) that solves the bacterial transport equation (see Table 1). (Reprinted with permission from ref. 96. Copyright 2010 American Chemical Society.)

terms of the bacterial chemotactic response. The spatial distribution of *E. coli* AW405 in the established gradient was measured by automated counting of individual cells through phase-contrast microscopy, and compared with that predicted from the bacterial transport equation (see Table 1) using previously published values of the Chemotactic Sensitivity Coefficient[7] (Fig. 13F and G). Accurate characterization of the concentration gradient, along with the quantitative agreement between chemotaxis experiments and theoretical predictions, places diffusion-based steady gradient generators on a

solid footing for future chemotaxis experiments, as well as highlighting potential pitfalls to be avoided in the design of similar devices.

The timescales between gradient establishment in the hydrogel layer and that in the test channel could be effectively decoupled in this class of devices. The gradient within the hydrogel layer forms over a time $T \sim L^2/D$, dictated by *horizontal* diffusion across the hydrogel layer between the feeder channels. By first allowing the gradient in the hydrogel layer to establish, and only subsequently injecting bacteria into the test channel, gradient establishment in the test channel can be rapidly achieved by *vertical* diffusion across the height H of the test channel. This only takes a time $T_H \sim H^2/D$, since the gradient is already established in the hydrogel layer underneath. Typically, $T_H \ll T$, since $H \ll L$. For example, in the device of Ahmed *et al.*,[96] $L = 1$ mm and $H = 50$ μm, yielding $T = 15$ min and $T_H = 4.5$ s (for $D = 5.5 \times 10^{-10}$ m^2 s^{-1}). Recently, Haessler *et al.*[99] also confirmed this gradient buffering capacity in the agarose layer by numerical simulation and experimental measurements using the device configuration of Cheng *et al.*[91] The rapid equilibration of the gradient in the 'test' channel after injection of the bacterial suspension ensures a considerably shorter transient. While this will not affect the steady-state response of bacteria, it greatly facilitates the study of the transient chemotaxis response by making it possible to measure the latter under steady gradient conditions during the remainder of the experiment.

Arbitrary-gradient generator

An innovative method to generate steady concentration profiles of arbitrary shape has been developed by Wu *et al.*,[97] using an agarose-based technique (Fig. 14A and B). This design was proposed before the agarose-based linear gradient generator of Cheng *et al.*,[91] but only recently applied to bacterial chemotaxis.[96] The method relies on the same basic principle used by Diao *et al.*[90] to generate a steady gradient, and makes use of agarose as the hydrogel, as in Cheng *et al.*[91] and Ahmed *et al.*[96] The novelty resides in using a test channel of arbitrary planar layout (Fig. 14C), instead of one that is parallel to the feeder channels. Because the concentration at each location in the test channel exactly mirrors that in the agarose directly underneath, appropriate spatial arrangement of the test channel enables the creation of arbitrarily shaped concentration profiles along the contour of the test channel (Fig. 14D). Consider a test channel whose centerline has an arbitrary shape $y(x)$, where x and y are the directions along and perpendicular to the feeder channels, respectively. Then, the concentration profile $C(s)$ and its gradient dC/ds along the test channel are $C(s) = G_O\int(1 + y_x^2)^{-1/2}ds$ and $dC/ds = G_O(1 + y_x^2)^{-1/2}$, respectively, where s is the coordinate along the centerline of the test channel, G_O is the concentration gradient within the agarose layer, and $y_x = dy/dx$.

The technique proposed by Wu *et al.*[97] promises to be very powerful, because stable, shear-free chemoeffector profiles of arbitrary shape can be generated. A proof-of-concept application to surface-adherent cells was given by Abhyankar *et al.*[98] using an exponential gradient. Ahmed *et al.*[96] recently applied a modified version of this technique to bacterial chemotaxis. The modifications are the same ones described above for the linear gradient experiments of Ahmed *et al.*,[96] namely the relative vertical arrangement of test and feeder channels and the use of continuous flow in the feeder channels. Ahmed *et al.*[96] measured the bacterial distribution along the centerline of the test channel for both an exponential and a peaked concentration profile (Fig. 15A and B), by automated counting of individual cells. Measured distributions (Fig. 15C and D) were in good agreement with those predicted by the bacterial transport equation (Fig. 15E and F), providing the first case of a bacterial chemotaxis study in steady nonlinear gradients.

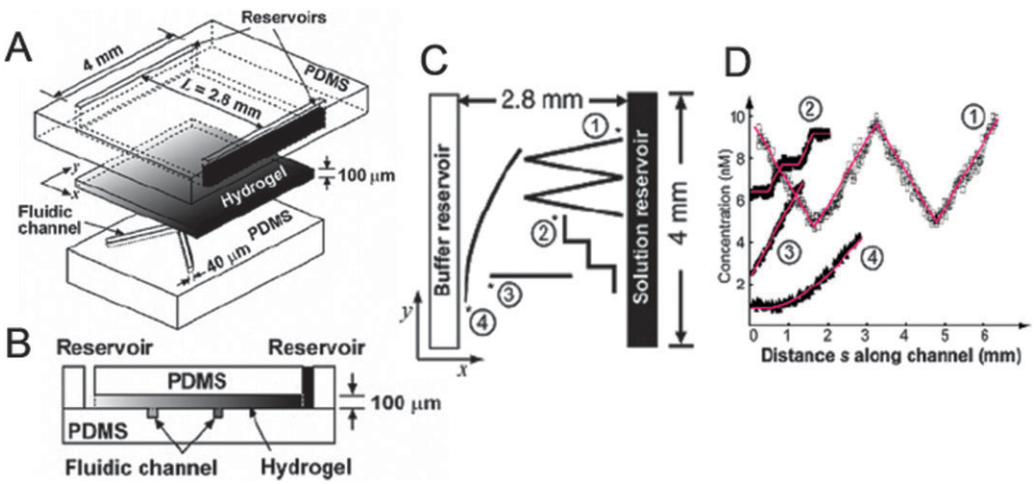

Fig. 14 The arbitrary-gradient generator of Wu *et al.*[97] (A) A 100 μm thick agarose layer is sandwiched between two PDMS layers. (B) The top PDMS layer contains the feeder reservoirs, which generate a steady gradient in the agarose layer, while the bottom layer contains the test channel ('fluidic channel'). The concentration at each point of the test channel mirrors that in the underlying agarose. (C) The test channel can have an arbitrary planar layout. Four configurations are shown. (D) When fluid in the test channel is quiescent, solute concentrations rapidly equilibrate with the gradient in the agarose layer above, so that the shape of the test channel determines the concentration profile along its contour. Symbols represent concentrations measured with confocal laser scanning microscopy, solid lines are predictions. Because the gradient in the agarose is steady, so is the concentration profile in the test channel. (Reprinted with permission from ref. 97. Copyright 2006 American Chemical Society).

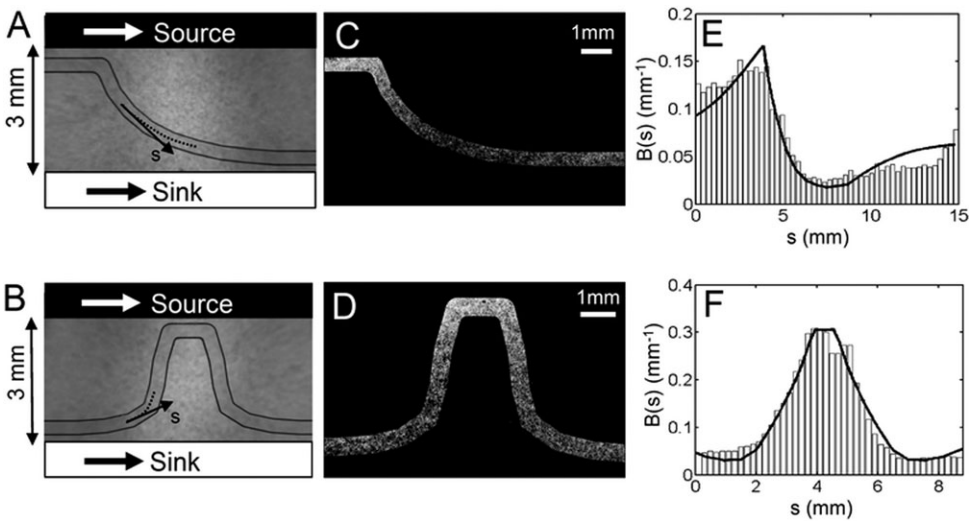

Fig. 15 **The arbitrary-gradient generator of Ahmed *et al.*[96]** (A, B) Using the principle described in Fig. 14, Ahmed *et al*. have fabricated and applied devices that create (A) exponential and (B) peaked concentration profiles, $C(s)$, where s is the coordinate along the contour of the test channel. Flow is constantly maintained in the feeder channels (source and sink), to ensure a steady concentration gradient in the underlying agarose layer (not shown) and, therefore, in the test channel. (C, D) Response of *E. coli* AW405 to (C) an exponential and (D) a peaked concentration profile of α-methylaspartate. Each image is a composite of multiple fields of view. Trajectories reveal strong accumulation of cells in the highest concentration region. (E, F) Normalized distribution of *E. coli* cells along the test channel, $B(s)$, from the experiments (bars) and the numerical model (lines). The latter is the solution of the bacterial transport equation (see Table 1) for two sets of chemotaxis parameter values (see ref. 7 for details). (Reprinted with permission from ref. 96. Copyright 2010 American Chemical Society.)

Evaluation of diffusion-based steady gradient generators

We believe that diffusion-based steady gradient generators that use hydrogels to mediate chemoeffector diffusion while preventing flow represent the most promising and versatile approach to study bacterial chemotaxis. The steadiness of the gradient is a very favorable feature, enabling chemotaxis studies over long timescales and observation of steady-state behavior and cell distributions. The gradients can be accurately characterized by confocal laser scanning microscopy and mathematical modeling.[96] The setup allows for multiple simultaneous gradients, parallel or antiparallel.[92,95] Although a rather long time (minutes to hours, depending on the dimensions of the device and diffusivity of chemoeffector) is required to establish the gradient in the hydrogel, chemotaxis experiments can be conveniently performed after (rather than during) gradient setup.[96] In this respect, gradient generation becomes another step of the fabrication and setup process, rather than an integral part of the experiment itself. This decoupling enables one to extend the use of such devices to the study of the transient responses of a bacterial population to a steady chemoeffector gradient, thereby enabling the characterization of transient and steady-state responses within a single experiment.

Microfluidic palette

In closing, we describe a recent diffusion-based device that does not immediately fit any of the previous classifications. This device, called 'microfluidic palette', uses the source-sink reservoir principle to generate multiple gradients within a 1.5 mm diameter circular chamber, by means of chemoeffectors transported *via* three feeder channels[49] (Fig. 16A–D). Since the feeder channels are directly connected with the observation chamber, without any barrier that prevents advection (such as a hydrogel), operation of this device requires careful balance of pressures in the feeder channels to avoid flow in the observation chamber. Provided this is achieved, this device can generate a two-dimensional steady gradient in a shear-free environment. The main feature of this device is that it allows for the quick switching of chemicals in the three feeder channels, to dynamically alter the chemical gradient during experiments. Its potential limitations include the rather complex shape of the gradient and the possibility for bacteria to escape from the observation chamber *via* the access ports, since no barrier to motility is present. This device was tested with *Pseudomonas aeruginosa* PAO1, a biofilm forming bacterium, which was found to follow glucose gradients as the glucose concentration was switched (Fig. 16E and F). While the characterization of the bacterial response to the transient gradients that form during switching will be complex, the ability to switch gradients could represent a novel feature that increases the arsenal of microfluidic devices for the study of bacterial chemotaxis.

8. Future directions

Although studies of surface-adherent cells and freely swimming cells impose different requirements on microfluidic chemotaxis devices, as discussed above, significant overlap exists. For example, early bacterial chemotaxis assays were mostly flow-based, and these continue to be useful for certain studies. On the other hand, diffusion-based gradient generators are becoming more popular for studies of motile surface-adherent cells[91,98,100,101] or even non-motile non-adherent cells like yeast,[102] primarily because they provide a more controlled biochemical environment and entirely avoid confounding effects of flow, either

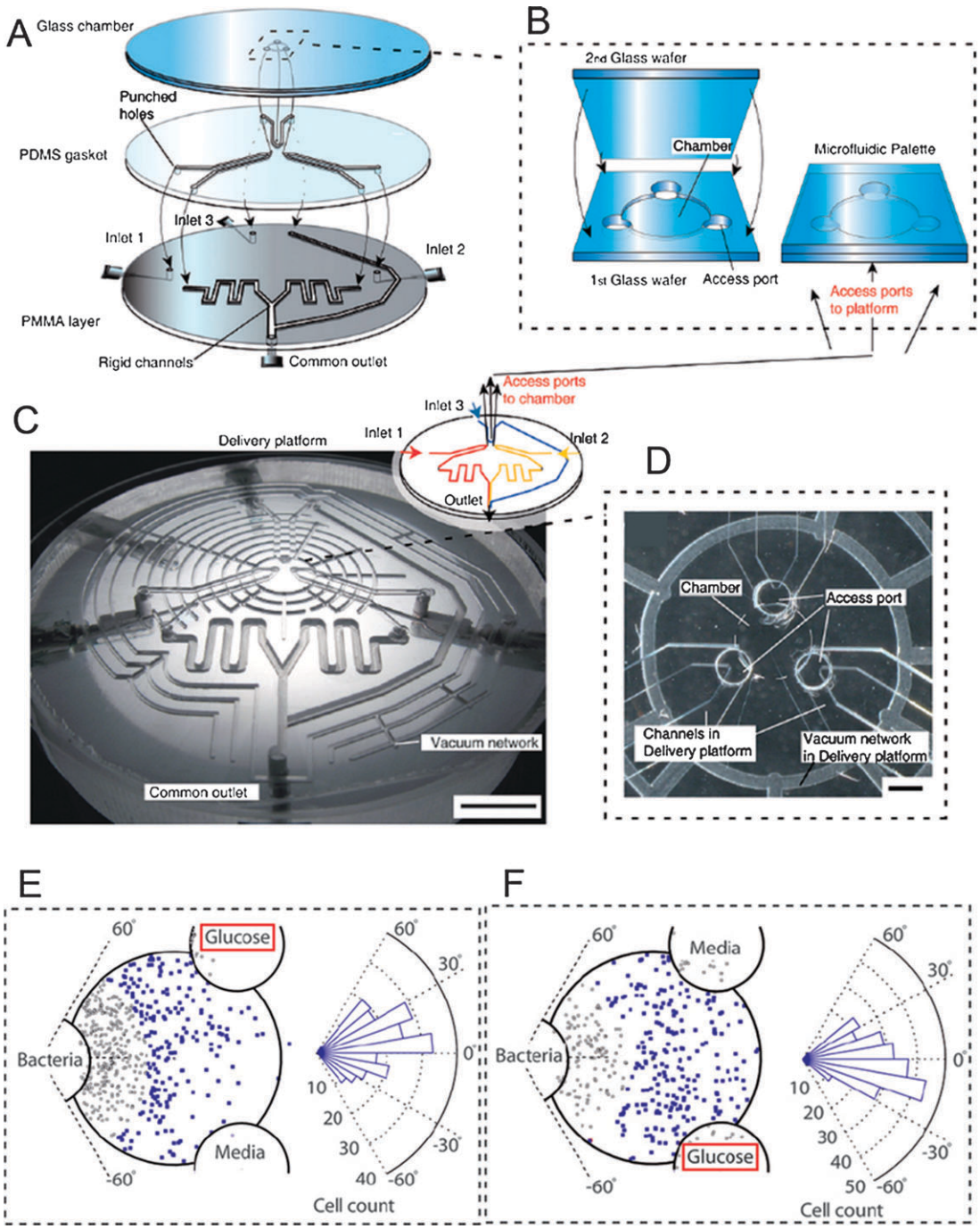

Fig. 16 **The microfluidic palette of Atencia *et al.*** [49] (A, B) A circular observation chamber is etched in a glass wafer, along with access ports. The chemoeffector is transported by three feeder channels fabricated in the PDMS gasket, underneath the glass wafer. The feeder channels have three separate inlets but a common outlet, constructed in the polymethylmethacrylate (PMMA) layer underneath. All three layers (glass, PDMS and PMMA) are reversibly bonded. (C, D) Photographs of the device further show the vacuum network constructed in the PMMA layer to enhance the seal between the PDMS and PMMA layers. (E) A two-dimensional glucose gradient is generated in the observation chamber by diffusion when glucose is introduced from one port, while the remaining two contain media. *Pseudomonas aeruginosa* (blue dots) moved towards the glucose source, and (F) followed it when the glucose source was switched. Grey dots are attached cells. (Reproduced from ref. 49 with permission. Copyright 2009 The Royal Society of Chemistry).

as hydrodynamic forces on cells or as convective transport of chemical signals. Surface-adherent cells *in vivo* might not experience flows[49] and flow could alter cellular response by removing locally generated chemical cues, like autocrine and paracrine signals,[91] and bias the direction of cellular migration.[82]

In the case of bacterial chemotaxis, flow could mimic an important aspect of the cells' natural environment, as in the case of the human gastrointestinal tract,[5] in a groundwater environment,[77] or for particle plumes in the ocean.[13] In these instances, it is important to ensure that flow

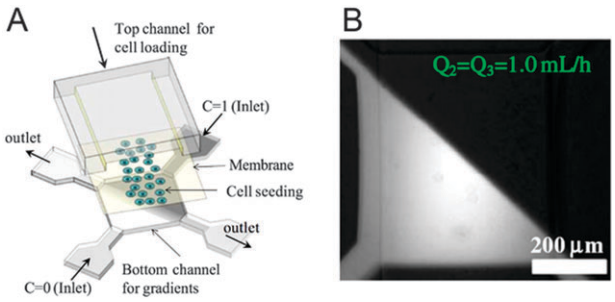

Fig. 17 The shear-free gradient generator of Kim *et al.*[103] (A) This hybrid design couples the advantages of rapid gradient generation by flow and gradient steadiness achieved by diffusion. A lower set of channels creates a chemoeffector gradient by flow. This gradient is transferred through a 10 µm polycarbonate membrane to a test chamber above, where fluid is quiescent. As long as the flow underneath is maintained steady, so is the gradient in the test chamber. (B) Kim *et al.*[103] used this device with two impinging streams of different concentration, resulting in a step-like gradient across the diagonal of the test chamber above. This was visualized using fluorescent dye (Rhodamine-B, 400 Da). The device was tested only with surface-adherent cells (HeLa), but is highly promising for application to bacterial chemotaxis. (With kind permission from Springer Science + Business Media: ref. 103, Fig. 1 and 2).

rates are commensurate with those found in the natural environment.

On the other hand, recent studies[92,95] have already begun to demonstrate the great potential of diffusion-based steady-gradient generators in furthering our understanding of the mechanistic basis and functional design of chemotaxis systems. Key advantages are the ability of these devices to decouple chemical stimuli from mechanical ones, as well as the stabilization of stimulus profiles during analyses of time-dependent chemotactic responses. In short, these devices provide a highly controlled environment, the possibility to conduct long experiments, and the ability to appropriately capture the transient response to steady chemical signals.

A disadvantage of diffusion-based steady-gradient generators is the long time required to set up gradients, particularly for large test channels, since gradient formation time increases quadratically with the distance between the source and sink reservoirs. On the other hand, flow-based gradient generators can create arbitrary gradients rapidly. Kim *et al.*[103] have combined the advantages of flow-based and diffusion-based gradient generators, by using flow to rapidly generate a gradient and diffusion through a polycarbonate membrane to transfer the gradient to a flow-free test chamber (Fig. 17A). The similarity between this device and those proposed by Ahmed *et al.*[96] is that vertical diffusion rapidly sets up a gradient in a shallow test chamber, once an underlying concentration profile is established. The advantage of the device of Kim *et al.*[103] is that the underlying concentration profile is also generated very rapidly, by flow instead of by horizontal diffusion. Kim *et al.*[103] applied this device to generate step-like concentration profiles with two impinging flows (Fig. 17B) and tested this configuration with surface-adherent cells. This

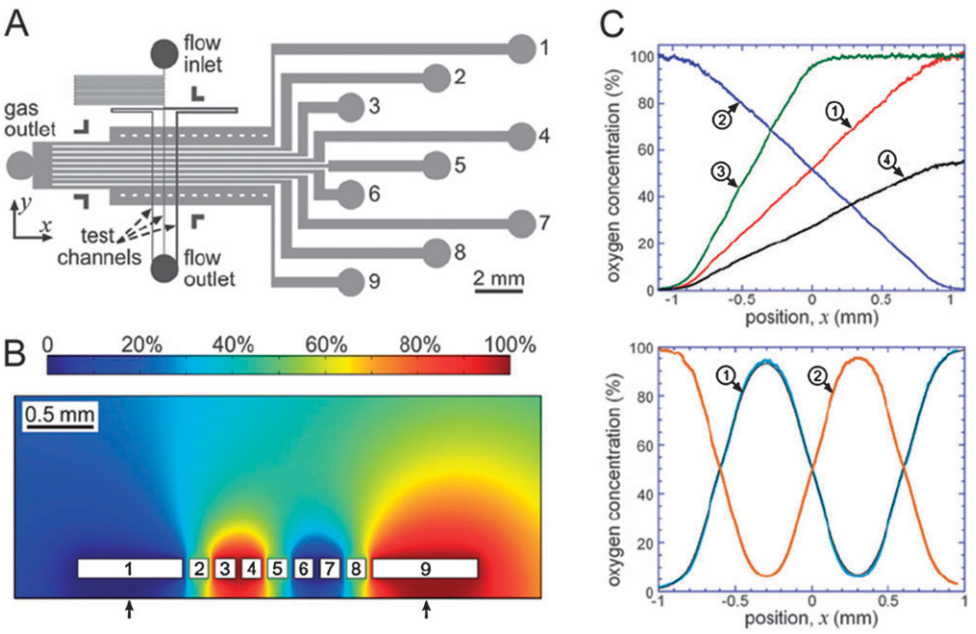

Fig. 18 The oxygen gradient generator of Adler *et al.*[104] (A) Using nine channels fabricated in PDMS that contain different oxygen concentrations, this device can generate arbitrarily shaped oxygen profiles. Vertical diffusion of oxygen from the nine channels through a 120 µm thick PDMS membrane transfers the gradient into the 3 test channels below. (B) Numerically simulated steady-state oxygen concentration, in percentage of the saturation value, within a vertical cross section in the PDMS just above a test channel, when different oxygen concentrations are flowed in the gas channels (here the gas channels 1,6,7 contained 0% O_2; 2,5,8 contained 50% O_2; 3,4,9 contained 100% O_2). (C) Measured oxygen concentration profiles along the longitudinal section of the test channel in a region bounded by the two arrows in B, as evaluated from the fluorescence of an oxygen-sensitive fluorescent dye, Ruthenium tris(2,20-dipyridyl) dichloride hexahydrate (RTDP). Different gradients can be produced by selecting appropriate oxygen concentrations in the gas channels. (Reproduced from ref. 104 with permission. Copyright 2010 The Royal Society of Chemistry).

hybrid technique is an important addition to the arsenal of microfluidic gradient generators and, while not applied to bacterial chemotaxis yet, it promises to extend the range of microfluidic studies on bacteria, particularly when temporally varying gradients are concerned. In this respect, this technique could provide a more flexible approach to 'switching gradients' compared to the 'microfluidic palette',[49] as it provides faster switching (flow-based rather than diffusion-based) and the ability to generate a broader set of gradients using previously developed flow-based device.

Yet other approaches enable one to study different tactic responses of bacteria. A recent example is the oxygen gradient generator of Adler *et al.*[104] This device exploits the permeability of PDMS to oxygen to generate arbitrarily shaped oxygen gradients. A number of microchannels flowing oxygen at desired concentrations are arranged directly above a test channel containing liquid (Fig. 18A), from which they are separated by a thin PDMS membrane. Oxygen permeates through the PDMS and diffuses into the liquid (Fig. 18B), and the oxygen concentration profile can elegantly be measured using an oxygen-sensitive fluorescent dye (Fig. 18C). Devices like this have great potential for fundamental studies on bacterial tactic responses, since many species of bacteria are aerotactic and some transition between motile and non-motile states depending on oxygen concentration.[105]

9. Conclusions

In the field of bacterial chemotaxis, like in many other research areas, the use of microfluidics is becoming commonplace not only in engineering and physics laboratories, but also in the hands of biologists. Concomitantly, technological innovations are increasingly being driven by the scientific questions at hand, and this tight integration between development and application has already begun to bear fruits in innovative studies of important open questions in chemotaxis.

Essential to this integration is a fundamental understanding of the technology, such that the best approach can be selected once a scientific question has been defined. We have provided an overview of the arsenal of microdevices now available to study bacterial chemotaxis, with an effort to highlight the relatively small number of physical and operational principles on which they are based. Flow-based devices are the tool of choice if the effects of flow represent an integral part of the question at hand. Unsteady diffusion-based gradient generators are ideal when the gradients that bacteria experience in their natural environment are ephemeral. Steady gradient generators offer excellent control in addressing questions concerning the design of cellular signaling circuits and the molecular underpinnings of bacterial chemotaxis. All of these devices benefit from the reproducibility and precision of microfluidics. Additionally, the flexibility of the microfabrication process offers immense possibilities for recreating salient features of natural bacterial environments (*e.g.* flow in porous media, particle settling) to study the ecological implications of chemotaxis.

Undoubtedly, the microfluidic toolbox for bacterial chemotaxis studies will continue to grow, as novel approaches for gradient generation emerge. Simultaneously, however, we must strive for a deeper and more widespread integration of technology and biology, so that each innovation can go beyond being merely an engineering marvel to become an enabling technology of new scientific discovery.

Acknowledgements

TA was partially supported by a Martin Fellowship for sustainability. TSS was supported by NWO/FOM. This work was also partially supported by NIH grant 1-R21-EB008844 and NSF grant OCE-0744641-CAREER to RS and by a grant from the Hayashi Fund from MIT's MISTI program.

References

1 G. Drews, *Photosynth. Res.*, 2005, **83**, 25–34.
2 M. S. Pittman, M. Goodwin and D. J. Kelly, *Microbiology*, 2001, **147**, 2493–2504.
3 M. B. Hugdahl, J. T. Beery and M. P. Doyle, *Infect. Immun.*, 1988, **56**, 1560–1566.
4 R. Freter and P. C. M. O'Brien, *Infect. Immun.*, 1981, **34**, 215–221.
5 D. L. Englert, M. D. Manson and A. Jayaraman, *Appl. Environ. Microbiol.*, 2009, **75**, 4557–4564.
6 R. O'Toole, S. Lundberg, S. A. Fredriksson, A. Jansson, B. Nilsson and H. Wolf-Watz, *J. Bacteriol.*, 1999, **181**, 4308–4317.
7 T. Ahmed and R. Stocker, *Biophys. J.*, 2008, **95**, 4481–4493.
8 S. Pandya, P. Iyer, V. Gaitonde, T. Parekh and A. Desai, *Curr. Microbiol.*, 1999, **38**, 205–209.
9 G. Pandey and R. K. Jain, *Appl. Environ. Microbiol.*, 2002, **68**, 5789–5795.
10 F. Azam, T. Fenchel, J. G. Field, J. S. Gray, L. A. Meyerreil and F. Thingstad, *Mar. Ecol.: Prog. Ser.*, 1983, **10**, 257–263.
11 N. Blackburn, F. Azam and A. Hagstrom, *Limnol. Oceanogr.*, 1997, **42**, 613–622.
12 J. R. Seymour, R. Simó, T. Ahmed and R. Stocker, *Science*, 2010, **329**, 342–345.
13 R. Stocker, J. R. Seymour, A. Samadani, D. E. Hunt and M. F. Polz, *Proc. Natl. Acad. Sci. U. S. A.*, 2008, **105**, 4209–4214.
14 F. Azam, *Science*, 1998, **280**, 694–696.
15 T. Fenchel and N. Blackburn, *Protist*, 1999, **150**, 325–336.
16 F. Azam and R. A. Long, *Nature*, 2001, **414**, 495–498.
17 H. C. Berg and D. A. Brown, *Nature*, 1972, **239**, 500–504.
18 H. Szurmant and G. W. Ordal, *Microbiol. Mol. Biol. Rev.*, 2004, **68**, 301–319.
19 G. H. Wadhams and J. P. Armitage, *Nat. Rev. Mol. Cell Biol.*, 2004, **5**, 1024–1037.
20 H. C. Berg, *E. coli in motion*, Springer-Verlag, 2003.
21 J. E. Segall, M. D. Manson and H. C. Berg, *Nature*, 1982, **296**, 855–857.
22 V. Sourjik and H. C. Berg, *Proc. Natl. Acad. Sci. U. S. A.*, 2002, **99**, 12669–12674.
23 J. E. Segall, S. M. Block and H. C. Berg, *Proc. Natl. Acad. Sci. U. S. A.*, 1986, **83**, 8987–8991.
24 U. Alon, M. G. Surette, N. Barkai and S. Leibler, *Nature*, 1999, **397**, 168–171.
25 N. Barkai and S. Leibler, *Nature*, 1997, **387**, 913–917.
26 D. Bray, M. D. Levin and C. J. Morton-Firth, *Nature*, 1998, **393**, 85–88.
27 V. Sourjik and H. C. Berg, *Proc. Natl. Acad. Sci. U. S. A.*, 2002, **99**, 123–127.
28 T. S. Shimizu, Y. Tu and H. C. Berg, *Mol. Syst. Biol.*, 2010, **6**, 382.
29 Y. Tu, T. S. Shimizu and H. C. Berg, *Proc. Natl. Acad. Sci. U. S. A.*, 2008, **105**, 14855–14860.
30 M. J. Schnitzer, *Phys. Rev. E*, 1993, **48**, 2553–2568.
31 D. A. Clark and L. C. Grant, *Proc. Natl. Acad. Sci. U. S. A.*, 2005, **102**, 9150–9155.
32 A. Celani and M. Vergassola, *Proc. Natl. Acad. Sci. U. S. A.*, 2010, **107**, 1391–1396.

33 L. Jiang, Q. Ouyang and Y. Tu, *PLoS Comput. Biol.*, 2010, **6**, e1000735.
34 D. Bray, M. D. Levin and K. Lipkow, *Curr. Biol.*, 2007, **17**, 12–19.
35 P. G. de Gennes, *Eur. Biophys. J.*, 2004, **33**, 691–693.
36 N. Vladimirov, L. Lovdok, D. Lebiedz and V. Sourjik, *PLoS Comput. Biol.*, 2008, **4**, e1000242.
37 M. J. Schnitzer, S. M. Block, H. C. Berg and E. M. Purcell, *Symp. Soc. Gen. Microbiol.*, 1990, **46**, 15–33.
38 J. Shioi, S. Matsuura and Y. Imae, *J. Bacteriol.*, 1980, **144**, 891–897.
39 Y. Magariyama, S. Sugiyama and S. Kudo, *FEMS Microbiol. Lett.*, 2001, **199**, 125–129.
40 M. L. Worku, R. L. Sidebotham, J. H. Baron, J. J. Misiewicz, R. P. H. Logan, T. Keshavarz and Q. N. Karim, *Eur. J. Gastroenterol. Hepatol.*, 1999, **11**, 1143–1150.
41 J. G. Mitchell and K. Kogure, *FEMS Microbiol. Ecol.*, 2006, **55**, 3–16.
42 J. G. Mitchell, L. Pearson, A. Bonazinga, S. Dillon, H. Khouri and R. Paxinos, *Appl. Environ. Microbiol.*, 1995, **61**, 877–882.
43 T. Fenchel and R. Thar, *FEMS Microbiol. Ecol.*, 2004, **48**, 231–238.
44 T. Fenchel, *Microbiology*, 1994, **140**, 3109–3116.
45 J. P. Armitage and R. M. Macnab, *J. Bacteriol.*, 1987, **169**, 514–518.
46 J. R. Seymour, T. Ahmed and R. Stocker, *J. Plankton Res.*, 2009, **31**, 1557–1561.
47 J. R. Seymour, Marcos and R. Stocker, *Am. Nat.*, 2009, **173**, E15–E29.
48 J. R. Seymour, T. Ahmed, W. M. Durham and R. Stocker, *Aquat. Microb. Ecol.*, 2010, **59**, 161–168.
49 J. Atencia, J. Morrow and L. E. Locascio, *Lab Chip*, 2009, **9**, 2707–2714.
50 J. Adler, *Science*, 1969, **166**, 1588–1597.
51 R. M. Ford, B. R. Phillips, J. A. Quinn and D. A. Lauffenburger, *Biotechnol. Bioeng.*, 1991, **37**, 647–660.
52 A. M. J. Law and M. D. Aitken, *Appl. Environ. Microbiol.*, 2005, **71**, 3137–3143.
53 H. C. Berg and L. Turner, *Biophys. J.*, 1990, **58**, 919–930.
54 J. Adler, *Science*, 1966, **153**, 708–716.
55 M. Silverman and M. Simon, *Nature*, 1974, **249**, 73–74.
56 R. K. Jain and J. Pandey, *Handbook of Hydrocarbon and Lipid Microbiology*, Springer-Verlag, Berlin, 2010.
57 D. L. Englert, A. Jayaraman and M. D. Manson, *Methods Mol. Biol.*, 2009, **571**, 1–23.
58 R. M. Ford and D. A. Lauffenburger, *Biotechnol. Bioeng.*, 1991, **37**, 661–672.
59 M. A. Rivero, R. T. Tranquillo, H. M. Buettner and D. A. Lauffenburger, *Chem. Eng. Sci.*, 1989, **44**, 2881–2897.
60 M. G. Vicker, *Exp. Cell Res.*, 1981, **136**, 91–100.
61 S. Saleh-Lakha and J. T. Trevors, *J. Microbiol. Methods*, 2010, **82**, 108–111.
62 G. M. Whitesides, E. Ostuni, S. Takayama, X. Y. Jiang and D. E. Ingber, *Annu. Rev. Biomed. Eng.*, 2001, **3**, 335–373.
63 C. T. Culbertson, S. C. Jacobson and J. M. Ramsey, *Talanta*, 2002, **56**, 365–373.
64 P. Lewus and R. M. Ford, *Biotechnol. Bioeng.*, 2001, **75**, 292–304.
65 S. Wright, B. Walia, J. S. Parkinson and S. Khan, *J. Bacteriol.*, 2006, **188**, 3962–3971.
66 M. M. Wu, J. W. Roberts, S. Kim, D. L. Koch and M. P. DeLisa, *Appl. Environ. Microbiol.*, 2006, **72**, 4987–4994.
67 D. Irimia and M. Toner, *Lab Chip*, 2006, **6**, 345–352.
68 N. L. Jeon, H. Baskaran, S. K. W. Dertinger, G. M. Whitesides, L. Van de Water and M. Toner, *Nat. Biotechnol.*, 2002, **20**, 826–830.
69 W. Saadi, S. J. Wang, F. Lin and N. L. Jeon, *Biomed. Microdevices*, 2006, **8**, 109–118.
70 H. B. Mao, P. S. Cremer and M. D. Manson, *Proc. Natl. Acad. Sci. U. S. A.*, 2003, **100**, 5449–5454.
71 T. M. Keenan and A. Folch, *Lab Chip*, 2008, **8**, 34–57.
72 J. Adler, *J. Gen. Microbiol.*, 1973, **74**, 77–91.
73 L. M. Lanning, R. M. Ford and T. Long, *Biotechnol. Bioeng.*, 2008, **100**, 653–663.
74 I. Strauss, P. D. Frymier, C. M. Hahn and R. M. Ford, *AIChE J.*, 1995, **41**, 402–414.
75 F. W. Dahlquist, R. A. Elwell and P. S. Lovely, *J. Supramol. Struct.*, 1976, **4**, 329–342.
76 R. Jasuja, J. Keyoung, G. P. Reid, D. R. Trentham and S. Khan, *Biophys. J.*, 1999, **76**, 1706–1719.
77 T. Long and R. M. Ford, *Environ. Sci. Technol.*, 2009, **43**, 1546–1552.
78 W. R. DiLuzio, L. Turner, M. Mayer, P. Garstecki, D. B. Weibel, H. C. Berg and G. M. Whitesides, *Nature*, 2005, **435**, 1271–1274.
79 E. Lauga, W. R. DiLuzio, G. M. Whitesides and H. A. Stone, *Biophys. J.*, 2006, **90**, 400–412.
80 G. B. Jeffery, *Proc. Royal Soc. London*, 1922, **120**, 161–179.
81 Marcos and R. Stocker, *Limnol. Oceanogr.: Methods*, 2006, **4**, 392–398.
82 G. M. Walker, J. Q. Sai, A. Richmond, M. Stremler, C. Y. Chung and J. P. Wikswo, *Lab Chip*, 2005, **5**, 611–618.
83 J. T. Locsei and T. J. Pedley, *Bull. Math. Biol.*, 2009, **71**, 1089–1116.
84 F. Azam and F. Malfatti, *Nat. Rev. Microbiol.*, 2007, **5**, 782–791.
85 N. Blackburn, T. Fenchel and J. Mitchell, *Science*, 1998, **282**, 2254–2256.
86 J. R. Seymour, T. Ahmed, Marcos and R. Stocker, *Limnol. Oceanogr.: Methods*, 2008, **6**, 477–488.
87 H. Jeon, Y. Lee, S. Jin, S. Koo, C. S. Lee and J. Y. Yoo, *Biomed. Microdevices*, 2009, **11**, 1135–1143.
88 F. Dahlquist, P. Lovely and D. Koshland, *Nature*, 1972, **236**, 120–123.
89 R. Mesibov, G. W. Ordal and J. Adler, *J. Gen. Physiol.*, 1973, **62**, 203–223.
90 J. P. Diao, L. Young, S. Kim, E. A. Fogarty, S. M. Heilman, P. Zhou, M. L. Shuler, M. M. Wu and M. P. DeLisa, *Lab Chip*, 2006, **6**, 381–388.
91 S. Y. Cheng, S. Heilman, M. Wasserman, S. Archer, M. L. Shuler and M. M. Wu, *Lab Chip*, 2007, **7**, 763–769.
92 Y. V. Kalinin, L. L. Jiang, Y. Tu and M. M. Wu, *Biophys. J.*, 2009, **96**, 2439–2448.
93 S. M. Block, J. E. Segall and H. C. Berg, *J. Bacteriol.*, 1983, **154**, 312–323.
94 B. A. Mello and Y. Tu, *Biophys. J.*, 2007, **92**, 2329–2337.
95 Y. Kalinin, S. Neumann, V. Sourjik and M. M. Wu, *J. Bacteriol.*, 2010, **192**, 1796–1800.
96 T. Ahmed, T. S. Shimizu and R. Stocker, *Nano Lett.*, 2010, **10**, 3379–3385.
97 H. K. Wu, B. Huang and R. N. Zare, *J. Am. Chem. Soc.*, 2006, **128**, 4194–4195.
98 V. V. Abhyankar, M. W. Toepke, C. L. Cortesio, M. A. Lokuta, A. Huttenlocher and D. J. Beebe, *Lab Chip*, 2008, **8**, 1507–1515.
99 U. Haessler, Y. Kalinin, M. A. Swartz and M. Wu, *Biomed. Microdevices*, 2009, **11**, 827–835.
100 C. W. Li, R. S. Chen and M. S. Yang, *Lab Chip*, 2007, **7**, 1371–1373.
101 B. Mosadegh, C. Huang, J. W. Park, H. S. Shin, B. G. Chung, S. K. Hwang, K. H. Lee, H. J. Kim, J. Brody and N. L. Jeon, *Langmuir*, 2007, **23**, 10910–10912.
102 S. Paliwal, P. A. Iglesias, K. Campbell, Z. Hilioti, A. Groisman and A. Levchenko, *Nature*, 2007, **446**, 46–51.
103 T. Kim, M. Pinelis and M. M. Maharbiz, *Biomed. Microdevices*, 2009, **11**, 65–73.
104 M. Adler, M. Polinkovsky, E. Gutierrez and A. Groisman, *Lab Chip*, 2010, **10**, 388–391.
105 C. Douarche, A. Buguin, H. Salman and A. Libchaber, *Phys. Rev. Lett.*, 2009, **102**, 198101.